

**DEVELOPMENT OF Q1 MIXED-INTERPOLATED
DISPLACEMENT/VELOCITY ELEMENTS FOR
SOLIDS AND FLUIDS**

by

Daniel Pantuso

Ingeniero Civil, Universidad de Buenos Aires, Argentina (1991)

Submitted to the Department of Mechanical Engineering
in partial fulfillment of the requirements
for the degree of

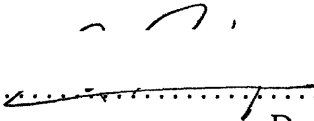
Master of Science in Mechanical Engineering

at the

MASSACHUSETTS INSTITUTE OF TECHNOLOGY

February 1995

© Massachusetts Institute of Technology 1995. All rights reserved.

Signature of Author 
Department of Mechanical Engineering
February, 1995

Certified by
Klaus-Jürgen Bathe
Professor of Mechanical Engineering
Thesis Supervisor

Accepted by
Eng. Ain Ants Sonin
Chairman, Graduate Committee

MASSACHUSETTS INSTITUTE
OF TECHNOLOGY

APR 06 1995

LIBRARIES

**DEVELOPMENT OF Q1 MIXED-INTERPOLATED
DISPLACEMENT/VELOCITY ELEMENTS FOR SOLIDS AND
FLUIDS**

by

Daniel Pantuso

Submitted to the Department of Mechanical Engineering
on February, 1995, in partial fulfillment of the
requirements for the degree of
Master of Science in Mechanical Engineering

Abstract

Low order standard finite element formulations fail when subjected to bending action and when nearly or totally incompressible situations are encountered. However, due to numerical advantages, it is very desirable to have a reliable and efficient low order element, in particular for 3-D analysis. This thesis presents a new low order element which is based on a mixed interpolation of displacements (velocities), pressure and strains (velocity strains). The proposed element shows promise for general compressible and incompressible analysis of solids and fluids. We show that the element passes a numerical inf-sup test, and give results to some standard analysis problems that demonstrate the capabilities of the element. We also explore other alternatives that can be considered in the selection of the pressure as well as the strain interpolations which fail to satisfy the inf-sup condition.

Thesis Supervisor: Klaus-Jürgen Bathe
Title: Professor of Mechanical Engineering

*To the memory of my father, Gerardo Pantuso,
who always encouraged me to continue my studies*

Acknowledgements

I would first like to express my warmest thanks to my wife, Alejandra, and my family whose love and encouragement constituted a priceless support.

I would also like to express my deep appreciation to Professor Klaus-Jürgen Bathe, my thesis supervisor, for his continuous guidance and unfailing support since my arrival to M.I.T. He has been an excellent teacher to me and has always shown a great interest throughout the course of this work.

I am very grateful to Professor Eduardo N. Dvorkin who introduced me to the field of Computational Mechanics and Solid Mechanics.

I am also thankful to my colleagues in the Finite Element Research Group at M.I.T. for their invaluable suggestions and assistance during the course of my research. Thanks also to many friends who have made my staying here an enjoyable one.

I also want to thank ADINA R&D, Inc. for allowing me to use their proprietary software - ADINA, ADINA-F, ADINA-IN and ADINA-PLOT - for this research work.

This research was supported by Professor Bathe's multi-sponsor project Analysis of Fluid-structure Interactions and since September 1994 by the Rocca Fellowship for which I am very grateful.

Contents

Titlepage	1
Abstract	2
Dedication	3
Acknowledgments	4
Contents	5
List of Figures	8
List of Tables	10
1 Introduction	11
2 Currently available low order elements	14
2.1 The u/p formulation	15
2.2 Assumed strain methods	17
2.3 Assumed stress methods	18
2.4 Other approaches	18
2.4.1 Penalty method	18
2.4.2 Augmented Formulations	18
2.4.3 Orthogonal Projections	19

3	Criterion for stability and convergence. The inf-sup condition	20
3.1	Incompressible elasticity	22
3.2	Spurious pressure modes	27
3.3	The inf-sup test	28
4	Development of the element	31
4.1	The new proposed element	31
4.1.1	Variational formulation	31
4.1.2	Implementation	35
4.1.3	The axisymmetric element	39
4.2	Implementation of the numerical inf-sup test	40
4.3	Other possibilities in the selection of interpolation fields	44
4.3.1	The enhanced strain field interpolation	45
4.3.2	Pressure interpolations. Internal degrees of freedom	48
4.3.3	The use of bubble functions	53
5	Numerical Tests	54
5.1	Beam Bending	54
5.2	No-Flow test	54
5.3	Driven Cavity	56
5.4	Convergence analysis	61
5.5	Axisymmetric cylinder under internal pressure	64
5.6	Thin cylinder under bending action	67
5.7	Circular plate under uniformly distributed load	68
6	Three-dimensional analysis	69
6.1	The three-dimensional element	69
6.2	Numerical results	71
6.2.1	Patch test	71
6.2.2	Beam bending	71

<i>Contents</i>	7
-----------------	---

7 Conclusions	73
----------------------	-----------

References	75
-------------------	-----------

List of Figures

2-1	Macro-element built with five Q1/P0 elements	16
3-1	Spaces considered to derive the inf-sup condition	25
4-1	Inf-sup test. Problems considered	40
4-2	Results of the inf-sup test for the constrained cavity shown in Figure 4.1. N is the number of elements per side of plate in Figure 4.1 and IS is the calculated inf-sup value	43
4-3	Results of the inf-sup test for the cantilever problem shown in Figure 4.1. N is the number of elements per side of plate in Figure 4.1 and IS is the calculated inf-sup value	44
4-4	Results of the inf-sup test using the strain interpolations defined in eqn. (4.47). N is the number of elements per side of plate in Figure 4.1 and IS is the calculated inf-sup value	48
4-5	Spurious pressure modes. Element discretization	50
4-6	Spurious pressure modes. Checkerboard distribution	50
4-7	Spurious pressure modes. Patch of four equal elements	52
5-1	Bending test. Poisson's ratio = 0	55
5-2	No-flow test	56
5-3	Driven cavity. Boundary condition at corner element	57
5-4	Driven cavity. Pressure distribution	58
5-4	Driven cavity. Pressure bands	59

5-4	Driven cavity. Pressure bands	60
5-5	Convergence analysis. Sequence of uniform meshes considered	62
5-6	Convergence analysis. Sequence of distorted meshes considered	62
5-7	Convergence analysis. Uniform mesh results	63
5-8	Convergence analysis. Distorted mesh results	63
5-9	Cylinder under internal pressure. Model considered	64
5-10	Cylinder under internal pressure. Convergence rates	66
5-11	Thin cylinder under bending action. Model considered	67
5-12	Circular plate under uniformly distributed load. Model considered . .	68
6-1	Patch test for 3-D analysis	72
6-2	Bending test for 3-D analysis. Poisson's ratio = 0	72

List of Tables

5-1	Cylinder under internal pressure. Results	65
5-2	Thin cylinder under bending action. Results	67
5-3	Circular plate under uniformly distributed load. Results	68

Chapter 1

Introduction

Much research effort has been spent to obtain an effective four-node quadrilateral finite element for the analysis of two-dimensional (or eight-node brick element for three-dimensional) structural problems and fluid flows. Low order elements are particularly attractive due to the fact that they are computationally more efficient than higher order elements. However, low order displacement-based formulations fail when subjected to bending action and also when nearly incompressible conditions are encountered [1].

To circumvent this problem many finite elements have been developed, with mixed formulations the most popular approach. Among them we can mention assumed strain formulations [2],[3],[4],[5], assumed stress formulations [6],[7] and the u/p formulation. In the first two cases, not only the displacement field but also the strain field or the stress field respectively are interpolated allowing an enhancement in the predictive capabilities of the element. The u/p formulation is also widely used. The latter is particularly attractive when dealing with constrained problems (incompressible analysis). In this scheme the displacement field and the pressure field are interpolated separately. Other approaches that have also received considerable attention are the Lagrange multiplier method, the penalty method, augmented formulations [8] and the method of orthogonal projections [9].

It is our purpose to develop a low order finite element formulation with high predictive capabilities under bending action and that does not exhibit locking behavior in the nearly incompressible limit. To this end we use the u/p formulation together with an enhancement of the strain field. In this context there exists many possibilities to select the pressure as well as the strain interpolations. In our formulation we specialize a Hellinger-Reissner variational indicator to obtain the algebraic finite element equations.

The mathematical condition that we would like our element to satisfy is the inf-sup condition for incompressible analysis [1],[10]. To investigate whether the element satisfies the inf-sup condition we have implemented a numerical inf-sup test that was first presented in [11].

The thesis is divided into seven chapters. Chapter 2 presents a review of currently available four-node quadrilateral elements. We briefly discuss their advantages and disadvantages as well as some features related to their formulation.

Chapter 3 summarizes basic concepts regarding the inf-sup condition, the presence of spurious pressure modes and the numerical inf-sup test. It is not our aim to go deeply into the theory of the inf-sup condition but to present some relevant issues related to the element implementation.

In chapter 4 we present the proposed element. We describe in detail the quadrilateral element for two-dimensional situations and give an extension for axisymmetric analysis. The numerical inf-sup test presented in chapter 3 is implemented and the obtained results for different test problems are shown. We also analyze in very detail other possible options for the selection of the pressure and strain field interpolations.

In chapter 5 the results of some standard numerical tests are shown that demonstrate the capabilities of the element. The behavior of the element under bending action and almost incompressible conditions is especially addressed. We also perform a numerical study to determine the order of convergence of the new element.

In chapter 6 we present a natural extension of our element to three-dimensional

analysis and give some numerical results.

Finally some conclusions are drawn in chapter 7.

Chapter 2

Currently available low order elements

There is a large number of low order elements available for the analysis of solids and fluids. The simplest one is the four-node displacement-based element, but, as is well known, this element does not yield sufficiently good results when subjected to bending action and also when nearly incompressible conditions are encountered. This phenomenon is usually referred to as “locking”. Because of the importance of having a reliable low order element, due to the ease of meshing and so on, many techniques have been developed to avoid the locking phenomenon.

Good results have been obtained to handle the shear locking behavior by using strain or stress assumed methods [2],[3],[4],[5],[6],[7]. An important improvement is also observed in almost incompressible situations with respect to the standard displacement-based element but pressure oscillations still appear in certain standard tests.

The u/p formulation is quite popular when dealing with incompressibility. In this context, the selection of the pressure interpolation plays a crucial role and the

stability of the model is highly dependent on it.

In what follows we briefly discuss the most popular methods currently available.

2.1 The u/p formulation

The formulation must satisfy the inf-sup condition in order to guarantee stability. The inf-sup condition will detect both, the locking phenomenon when the inf-sup expression is not bounded from below by a value $\beta > 0$ and the presence of spurious pressure modes which correspond to a zero value of the inf-sup expression.

Certain design criteria must be considered when choosing the interpolation functions. Roughly speaking, the main idea is to balance the displacement space and the pressure space to avoid the locking phenomenon and at the same time to maintain optimal rates of convergence.

A classical element that falls within this category is the well-known Q1/P0 element (see [10] for a very deep discussion regarding the behavior of this element). The displacement interpolations are those corresponding to the standard four-node isoparametric element and the pressure field is assumed to be constant throughout the element.

Although in the above mentioned Q1/P0 element the displacement and pressure spaces are correctly balanced, this formulation does not work for a general mesh. In fact, spurious pressure modes will be present in discretizations of equal-size square elements with certain boundary conditions (see [1], example 4.38). Even though this effect disappears when distorted elements are used, the element does not satisfy the inf-sup condition.

Actually, to satisfy the inf-sup condition it is necessary to employ higher order elements, namely Q2/P1 and Q3/P2 elements. It is also possible to prove stability on a mesh built of macro-elements as the one shown in Figure 2-1. Each macro-element is formed using Q1/P0 elements. Even though the inf-sup condition is satisfied, the use

of macro-elements is not quite popular. One of the reasons could be that models made of macro-elements are really expensive. Note that, in this case, each macro-element is built using five Q1/P0 elements.

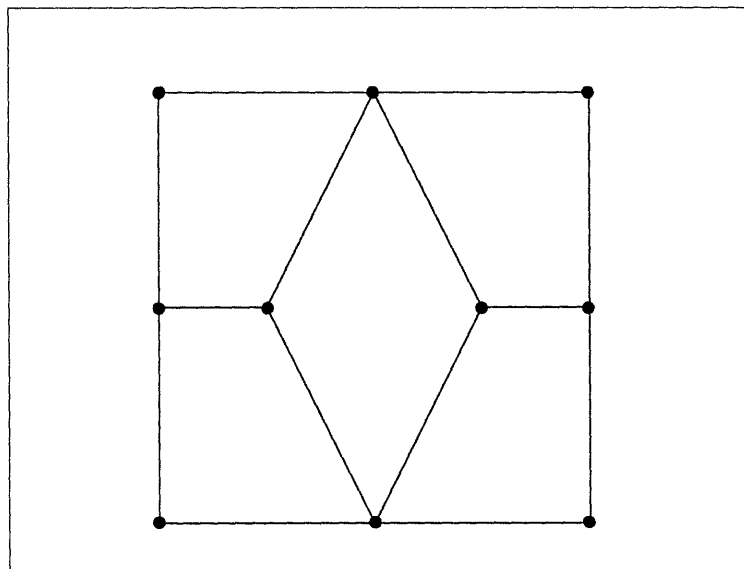


Figure 2-1: Macro-element built with five Q1/P0 elements

Choosing the same order for the interpolation of the displacement and pressure fields leads to undesirable results in the pressure distribution. Therefore, it is necessary to modify the displacement and pressure approximations in some way to obtain acceptable results. Hughes, Franca and Balestra proposed in [12] an element with linear displacement and pressure interpolations. They introduced a modification in the displacement interpolations by using a Petrov-Galerkin scheme. The formulation is stable and convergent, but results are dependent on the selection of an external parameter. Besides, a non-symmetric stiffness matrix is obtained which requires a special treatment in the solution of the resulting linear system of equations.

Zienkiewicz and Wu proposed in [13] other approaches to deal with incompressibility in the context of the u/p formulation.

2.2 Assumed strain methods

In standard finite element formulations, the strain field is usually determined through kinematic relations from the displacement field. When assumed strain methods are used, the strain field is modified in order to forbear locking behavior of the element. For example, to deal with shear locking the deviatoric part of the strain field must be modified, on the other hand, when incompressible situations are encountered the dilatational part is what we must change.

In [2] Hughes proposed a modification of the \mathbf{B} operator (which is directly obtained from the displacement interpolation) for the analysis of incompressible media by introducing an assumed \mathbf{B}^{dil} operator (also known as B-bar method). Different options to define the operator \mathbf{B}^{dil} can be considered. Among them we mention selective integration and the mean-dilatation formulation as the most widely used.

Bathe and Dvorkin [3] proposed a shell element in which the strain field is calculated from the displacement field at certain sampling points and then interpolated over the element. Therefore the actual strain field is defined at any location inside the element by interpolating using the strain values obtained at the sampling points. Based on the same ideas, a two-dimensional element was developed in [4].

Simo and Rifai introduced in [5] a general framework, derived from a Hu-Washizu principle, in which the strain field is given by the usual one derived from the displacement field plus the addition of an assumed enhanced strain field. The proposed element shows good behavior when subjected to bending action but some oscillations in the pressure field are present in incompressible analysis. It is also shown that the incompatible element of Wilson [14] can be recovered within this framework.

Assumed strain methods can usually be obtained from a variational formulation. However, sometimes the stress recovery is not variational consistent [15].

2.3 Assumed stress methods

They are based on a two-field variational formulation in which the displacement and stress field are interpolated separately. Since they are based on complementary-energy variational formulations, it is required that the assumed stress field satisfy a priori the equilibrium equations.

The works of Pian and Sumihara [6] and Punch and Atluri [7] fall within this approach.

The extension to non-linear analysis presents some difficulties. Constitutive equations generally relate the stress tensor to a suitable conjugate strain measure. While strain methods use this relation directly, stress methods use inverse constitutive relations. Furthermore, standard algorithms in non-linear mechanics are strain driven (i.e. radial return algorithm in plasticity) and must be modified when employed in the present context.

2.4 Other approaches

2.4.1 Penalty method

The penalty method has also been extensively used. Here, the displacements are considered as the basic variable and the problem consists in minimizing a modified functional. This modification introduces a large parameter that leads to ill-conditioning of the functional. Besides, locking behavior is present and some techniques, like for example reduced integration, must be implemented. More details can be found in [10] and references therein.

2.4.2 Augmented Formulations

Augmented formulations consist of weakening the divergence-free constraint by using

$$\operatorname{div}(\mathbf{u}_h) = g_h \quad (2.1)$$

Different forms have been proposed for g_h , see for example [8].

In general, the expression for g_h depends on an externally imposed parameter α and results are highly dependent on it. The main difficulty arises in finding the best value for α .

2.4.3 Orthogonal Projections

The method of orthogonal projections provides a way of solving a set of linear equations which are subjected to a certain number of linearly independent constraints. The idea consists of splitting the solution vector in the sum of two orthogonal vectors, one of which lies in the constrained space and the other in an orthogonal space to that. The major work is spent in the construction of the two projection orthogonal operators [16].

The same general idea can be applied in the context of the finite element method when certain restrictions hold (i.e. incompressibility). One of the projection operators is constructed by vectors that define the constrained space. The other is complementary in the sense that their sum is the identity matrix. A four-node quadrilateral element that uses this approach was presented in [9].

Chapter 3

Criterion for stability and convergence. The inf-sup condition

A large number of problems in engineering practice reduce to the minimization of a potential of the form

$$\Pi(\mathbf{v}) = \frac{1}{2} a(\mathbf{v}, \mathbf{v}) - f(\mathbf{v}) \quad \mathbf{v} \in V \quad (3.1)$$

If $a(\cdot, \cdot)$ is a continuous V -elliptic bilinear form and $f(\cdot)$ is a continuous linear form, the Lax-Milgram theorem assures that the minimization of $\Pi(\mathbf{v})$ has one and only one solution. To estimate the order of convergence, the Cea's lemma together with some results obtained from interpolation theory give [17]

$$\|\mathbf{u} - \mathbf{u}_h\|_j \leq C h^{k+1-j} |\mathbf{u}|_{k+1} \quad (3.2)$$

where \mathbf{u}_h is the finite element solution, k is the order of the polynomial used to interpolate \mathbf{u} and

$$\|\cdot\|_j^2 = \int_{\Omega} \sum_{\substack{m,n=1 \\ |k|\leq j}}^3 \left(\frac{\partial^k(\cdot)_m}{\partial x_n^k} \right)^2 d\Omega \quad (3.3)$$

$$|\cdot|_j^2 = \int_{\Omega} \sum_{m,n=1}^3 \left(\frac{\partial^j(\cdot)_m}{\partial x_n^j} \right)^2 d\Omega \quad (3.4)$$

What eqn. (3.2) tells us is that the rate of convergence of our finite element solution is governed by a constant C times a certain power of the element size, h . This power depends on the degree of the polynomial used in the approximations and gives the order of convergence of our formulation.

The constant C sometimes depends on the conditions of the problem. For example, if almost incompressible conditions are encountered, C will increase as the Poisson ratio $\nu \rightarrow 1/2$ and, as a consequence, the element will lock. Therefore, a stronger condition than those imposed by the Lax-Milgram theorem ought to be considered in order to decide whether a finite element model will have good convergence properties or not. In this context, the inf-sup condition, often referred to as the Brezzi-Babuška condition, arises as the criterion to be satisfied to assure stability.

The potential to be minimized is written now as,

$$\Pi(\mathbf{v}) = \frac{1}{2} a(\mathbf{v}, \mathbf{v}) + \frac{1}{2} \kappa b(\mathbf{v}, \mathbf{v}) - f(\mathbf{v}) \quad \mathbf{v} \in V \quad (3.5)$$

where both $a(\cdot, \cdot)$ and $b(\cdot, \cdot)$ stand for continuous bilinear forms and κ is a very large parameter.

Two fundamentally different types of problems can be analyzed within this framework,

- Constrained problems.
- Formulations in which the potential can be split into two parts and one of them is magnified by a large coefficient.

Some problems that fall within this category are elasticity problems in which nearly incompressible conditions are encountered, incompressible fluid flows and beams, plates and shells when the thickness is very small compared with the side dimensions. In what follows we refer to incompressible elasticity and results carry over immediately to the Stokes problem. The extension to beams, plates and shells is not straight forward. See [11] for the case of beams.

3.1 Incompressible elasticity

In incompressible elasticity the terms involved in eqn. (3.5) are

$$a(\mathbf{v}, \mathbf{v}) = 2G \int_{\Omega} \boldsymbol{\epsilon}'(\mathbf{v}) \cdot \boldsymbol{\epsilon}'(\mathbf{v}) \, d\Omega \quad (3.6)$$

$$b(\mathbf{v}, \mathbf{v}) = \int_{\Omega} (\operatorname{div} \mathbf{v})^2 \, d\Omega \quad (3.7)$$

$$f(\mathbf{v}) = \int_{\Omega} \mathbf{v} \cdot \mathbf{f}^B \, d\Omega + \int_{S_f} \mathbf{v}^{S_f} \cdot \mathbf{f}^{S_f} \, dS_f \quad (3.8)$$

where Ω is the volume over which integration is performed, $\boldsymbol{\epsilon}'(\mathbf{v})$ is the deviatoric part of the strain tensor, G and κ are the shear and bulk modulus respectively and \mathbf{f}^B and \mathbf{f}^{S_f} are the externally applied body forces and externally applied tractions. S_f is the portion of the boundary over which tractions are prescribed while we use S_u to denote that part over which displacements (velocities) are prescribed.

We are seeking the displacement field \mathbf{u} which minimizes eqn. (3.5) over a vectorial space V ,

$$V = \left\{ \mathbf{v} / \frac{\partial v_i}{\partial x_j} \in L^2(\Omega) ; i, j = 1..3 \text{ and } v_i|_{S_u} = 0 ; i = 1..3 \right\} \quad (3.9)$$

Let us now consider the discrete problem and let \mathbf{u}_h denote the approximate solution or finite element solution lying in the finite dimensional space V_h . Here, V_h stands for a space of a sequence of finite element spaces that we choose to solve the

problem,

$$V_h = \left\{ \mathbf{v}_h / \frac{\partial v_{i_h}}{\partial x_j} \in L^2(\Omega) ; i, j = 1..3 \text{ and } v_{i_h}|_{S_u} = 0 ; i = 1..3 \right\} \quad (3.10)$$

Therefore, each discrete problem

$$\min_{\mathbf{v}_h \in V_h} \left\{ \frac{1}{2} a(\mathbf{v}_h, \mathbf{v}_h) + \frac{\kappa}{2} b(\mathbf{v}_h, \mathbf{v}_h) - f(\mathbf{v}_h) \right\} \quad (3.11)$$

has a unique finite element solution \mathbf{u}_h .

We now define the distance between the exact solution \mathbf{u} and the finite element space V_h as

$$d(\mathbf{u}, V_h) = \inf_{\mathbf{v}_h \in V_h} \|\mathbf{u} - \mathbf{v}_h\| = \|\mathbf{u} - \tilde{\mathbf{u}}\| \quad (3.12)$$

where $\tilde{\mathbf{u}}$ is an element of V_h but is not necessarily the finite element solution.

Our purpose is to find conditions on V_h such that

$$\|\mathbf{u} - \mathbf{u}_h\| \leq c d(\mathbf{u}, V_h) \quad (3.13)$$

with the constant c independent of the conditions of the problem.

Since it is condition (3.13) which governs the good properties of our formulation, it is desirable to express it in other forms which are easier to work with. Thus, to proceed further we define the discrete spaces K_h and D_h

$$K_h(q_h) = \{ \mathbf{v}_h / \mathbf{v}_h \in V_h, \text{div } \mathbf{v}_h = q_h \} \quad (3.14)$$

$$D_h = \{ q_h / q_h = \text{div } \mathbf{v}_h \text{ for some } \mathbf{v}_h \in V_h \} \quad (3.15)$$

Note that in the limit, when κ is infinite, solutions must satisfy the incompress-

ibility constraint exactly. In particular, \mathbf{u}_h is constrained to lie in $K_h(0)$. Thus, if $K_h(0)$ is too small compared to V_h convergence could be affected. We are interested in having optimal convergence in our finite element analysis which means that, as the mesh is refined, the distance between \mathbf{u} and \mathbf{u}_h must remain of the same order of magnitude as $d(\mathbf{u}, V_h)$.

Since the limit case $\kappa \rightarrow \infty$ has the highest constraining effect we focus on it for our analysis. Then, as \mathbf{u}_h lies in V_h , optimal convergence cannot be guaranteed unless

$$d(\mathbf{u}, K_h(0)) \leq c d(\mathbf{u}, V_h) \quad (3.16)$$

Let \mathbf{u}_{h_0} be a vector in $K_h(0)$ and let \mathbf{w}_h be a vector such that

$$\tilde{\mathbf{u}}_h = \mathbf{u}_{h_0} + \mathbf{w}_h \quad (3.17)$$

Therefore, condition (3.16) is met provided that for all $q_h \in D_h$ there is a vector $\mathbf{w}_h \in K_h(q_h)$ such that

$$\|\mathbf{w}_h\| \leq c' \|q_h\| \quad (3.18)$$

where c' is an independent constant. Figure 3-1 shows schematically the spaces and vectors involved.

Suppose now that $c' = \frac{1}{\beta_h}$ is not independent of h . Hence, the distance between \mathbf{u} and $K_h(0)$ will not decrease at the same rate as $d(\mathbf{u}, V_h)$. However, convergence will still occur if $d(\mathbf{u}, V_h)$ decreases faster than β_h , though it will not be optimal.

Note that condition (3.18) is a strong guarantee for good convergence properties of our discretization.

The inf-sup condition follows now from (3.18) (see [1] for a nice derivation),

$$\inf_{q_h \in D_h} \sup_{\mathbf{v}_h \in V_h} \frac{\int_{\Omega} q_h \operatorname{div}(\mathbf{v}_h) \, d\Omega}{\|q_h\| \|\mathbf{v}_h\|_1} \geq \beta > 0 \quad (3.19)$$

If the inf-sup condition is satisfied for a sequence of finite element spaces, then our finite element discretization will exhibit the good approximation properties that we seek, namely, (3.13), (3.16) and (3.18) will all be satisfied.

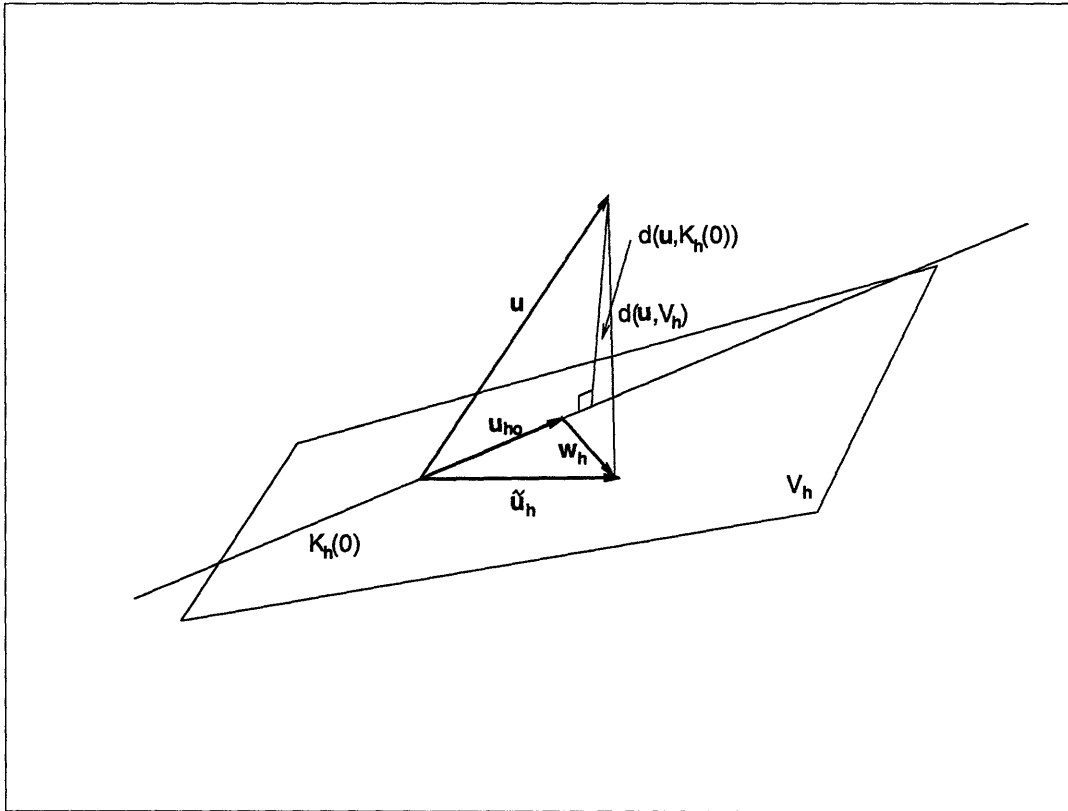


Figure 3-1: Spaces considered to derive the inf-sup condition

In practice, locking will be present when the potential Π defined in eqn. (3.5) is directly used. To circumvent this phenomenon, the u/p formulation appears as a convenient alternative and the following modified potential is used,

$$\Pi'(\mathbf{v}_h) = G \int_{\Omega} \boldsymbol{\epsilon}'(\mathbf{v}_h) \cdot \boldsymbol{\epsilon}'(\mathbf{v}_h) \, d\Omega + \frac{\kappa}{2} \int_{\Omega} (P_h(\operatorname{div} \mathbf{v}_h))^2 \, d\Omega - f(\mathbf{v}_h) \quad (3.20)$$

where $P_h(\cdot)$ is the L^2 -projector operator onto an auxiliary space Q_h which we identify as a pressure space. The projection operator is defined by,

$$\int_{\Omega} (P_h(\operatorname{div} \mathbf{u}_h) - \operatorname{div} \mathbf{u}_h) q_h \, d\Omega = 0 \quad \forall q_h \in Q_h \quad (3.21)$$

Invoking stationarity of $\Pi'(\mathbf{v}_h)$ we obtain

$$2G \int_{\Omega} \boldsymbol{\epsilon}'(\mathbf{u}_h) \cdot \boldsymbol{\epsilon}'(\mathbf{v}_h) \, d\Omega - \int_{\Omega} p_h \operatorname{div} \mathbf{v}_h \, d\Omega = f(\mathbf{v}_h) \quad \forall \mathbf{v}_h \in V_h \quad (3.22)$$

$$- \int_{\Omega} (\operatorname{div} \mathbf{u}_h + \frac{p_h}{\kappa}) q_h \, d\Omega = 0 \quad \forall q_h \in Q_h \quad (3.23)$$

and we infer from (3.23) that $p_h = -\kappa P_h(\operatorname{div} \mathbf{u}_h)$.

Let us now redefine $K_h(q_h)$ as

$$K'_h(q_h) = \{\mathbf{v}_h \in V_h / P_h(\operatorname{div} \mathbf{v}_h) = q_h\} \quad (3.24)$$

and the non-locking condition (3.16) becomes,

$$d(\mathbf{u}, K'_h(0)) \leq c d(\mathbf{u}, V_h) \quad (3.25)$$

The inf-sup condition now reads,

$$\inf_{q_h \in P_h(D_h)} \sup_{\mathbf{v}_h \in V_h} \frac{\int_V q_h \operatorname{div}(\mathbf{v}_h) \, dV}{\|q_h\| \|\mathbf{v}_h\|_1} \geq \beta > 0 \quad (3.26)$$

where the space D_h in eqn. (3.19) is replaced by $P_h(D_h)$. Therefore, in order to satisfy the inf-sup condition it is crucial how the space $P_h(D_h)$ relates to the displacement space V_h . Note that Q_h always contains $P_h(D_h)$. Choosing Q_h smaller renders $K'_h(0)$ larger leaving (3.25) easier to satisfy. However, taking $Q_h = \{0\}$, we have that $K'_h(0) = V_h$, and nothing remains for the incompressibility constraint. According to this, the key is to reduce Q_h sufficiently to avoid locking but keeping it as large

as possible for reasons of accuracy. On the other hand, using $P_h = I$ (the identity operator) the displacement-based formulation is recovered and the element locks.

Once the inf-sup condition is satisfied, the following error bounds can be shown to hold [18]

$$\|\mathbf{u} - \mathbf{u}_h\| \leq c_1 [\|\mathbf{u} - \mathbf{u}_I\| + \|(I - P_h)(p)\|] \quad (3.27)$$

$$\|p - \kappa P_h(\operatorname{div} \mathbf{u}_h)\| \leq c_2 [\|\mathbf{u} - \mathbf{u}_I\| + \|(I - P_h)(p)\|] \quad (3.28)$$

where c_1 and c_2 are independent constants.

3.2 Spurious pressure modes

In this section, we discuss some issues related to the presence of spurious pressure modes.

As mentioned above, in actual finite element discretizations we may well have $P_h(D_h)$ contained in but not equal to Q_h . Therefore, we must consider

$$\inf_{q_h \in Q_h} \sup_{\mathbf{v}_h \in V_h} \frac{\int_{\Omega} q_h \operatorname{div}(\mathbf{v}_h) \, d\Omega}{\|q_h\| \|\mathbf{v}_h\|_1} \geq \beta > 0 \quad (3.29)$$

instead of (3.26). In case $P_h(D_h) = Q_h$, (3.26) and (3.29) are exactly the same.

In case that the space Q_h is larger than the space $P_h(D_h)$, the solution will exhibit spurious pressure modes. They correspond to (non-zero) pressure distributions p_s that do not interact with the displacements. Thus, they satisfy,

$$\int_{\Omega} p_s \operatorname{div} \mathbf{v}_h \, d\Omega = 0 \quad \forall \mathbf{v}_h \in V_h \quad (3.30)$$

Assume now that we are given a pressure distribution \hat{p}_h which is proposed to be a spurious pressure mode. If $Q_h = P_h(D_h)$, there is always a vector $\hat{\mathbf{v}}_h$ such that

$\hat{p}_h = -P_h(\text{div}\hat{\mathbf{v}}_h)$ and

$$-\int_{\Omega} \hat{p}_h \text{div}\hat{\mathbf{v}}_h \, d\Omega = -\int_{\Omega} \hat{p}_h P_h(\text{div}\hat{\mathbf{v}}_h) \, d\Omega = \int_{\Omega} \hat{p}_h^2 \, d\Omega > 0 \quad (3.31)$$

On the other hand, when Q_h is larger than $P_h(D_h)$ we can find a pressure distribution in the space orthogonal to $P_h(D_h)$ which will satisfy (3.30).

Therefore, since we are testing with $q_h \in Q_h$, expression (3.29) tests whether any spurious pressure mode is present. Furthermore, when no spurious pressure modes are present, expression (3.29) tests if condition (3.26) is satisfied.

Spurious pressure modes can lead to large solution errors in case of totally incompressible situations or when prescribed displacements are different from zero. Further discussion on this topic can be found in [1],[11],[19].

3.3 The inf-sup test

It is not easy to determine whether a particular finite element formulation satisfies the inf-sup condition and only for a very few number of elements an analytical proof is available. See [1] for a review of existing elements. Thus, the numerical inf-sup test proposed in [11] appears as a very useful tool to predict if a certain discretization is likely to satisfy the inf-sup condition. Such a test can be applied to newly proposed elements and also to discretizations with elements of distorted geometries. However, we understand that this test, when passed, does not assure the satisfaction of the inf-sup condition, but, of course, if the numerical test is not passed that automatically means that the inf-sup condition is not satisfied.

To establish the basis of the inf-sup test, we consider the matrix problem associated with eqns. (3.22) and (3.23) for finite values of κ

$$\begin{bmatrix} \mathbf{A}_h & \mathbf{B}_h^T \\ \mathbf{B}_h & -\frac{1}{\kappa} \mathbf{T}_h \end{bmatrix} \begin{Bmatrix} \mathbf{U}_h \\ \mathbf{P}_h \end{Bmatrix} = \begin{Bmatrix} \mathbf{F}_h \\ \mathbf{0} \end{Bmatrix} \quad (3.32)$$

Clearly, from the last equation we have

$$\mathbf{B}_h \mathbf{U}_h - \frac{1}{\kappa} \mathbf{T}_h \mathbf{P}_h = \mathbf{0} \implies \frac{\mathbf{P}_h}{\kappa} = -\mathbf{T}_h^{-1} \mathbf{B}_h \mathbf{U}_h \quad (3.33)$$

and it follows that $-\mathbf{T}_h^{-1} \mathbf{B}_h$ is the matrix form associated with the linear operator $P_h(\text{div}(\cdot))$.

We can also write condition (3.26) in terms of nodal quantities instead of the fields. We note that having $q_h \in P_h(D_h)$ it is always possible to find \mathbf{w}_h such that $q_h = P_h(\text{div} \mathbf{w}_h)$. Thus, we obtain an all-displacement form of the inf-sup condition

$$\inf_{\mathbf{W}_h} \sup_{\mathbf{V}_h} \frac{\mathbf{W}_h^T \mathbf{G}_h \mathbf{V}_h}{\sqrt{\mathbf{W}_h^T \mathbf{G}_h \mathbf{W}_h} \sqrt{\mathbf{V}_h^T \mathbf{S}_h \mathbf{V}_h}} = \beta_h > 0 \quad (3.34)$$

where

$$\mathbf{V}_h^T \mathbf{S}_h \mathbf{V}_h = \int_V \sum_{i,j=1}^3 \frac{\partial v_{hi}}{\partial x_j} \frac{\partial v_{hi}}{\partial x_j} dV \quad (3.35)$$

$$\mathbf{W}_h^T \mathbf{G}_h \mathbf{V}_h = \int_V \text{div}(\mathbf{w}_h) P_h(\text{div} \mathbf{v}_h) dV \quad (3.36)$$

with \mathbf{S}_h a symmetric positive definite matrix and \mathbf{G}_h a symmetric positive semi-definite matrix.

The key is the evaluation of the inf-sup value of the expression in (3.34). To do that, the following eigenproblem must be considered.

$$\mathbf{G}_h \mathbf{V}_h = \lambda \mathbf{S}_h \mathbf{V}_h \quad (3.37)$$

Let us now call λ_p the first non-zero eigenvalue. Then, the inf-sup value is simply $\sqrt{\lambda_p}$ (see [11]) and we require that for any sequence of meshes this value remain bounded from below by a constant $\beta_h > 0$.

We can also detect the presence of spurious pressure modes in our formulation. Suppose that we have n_u displacement and n_p pressure degrees of freedom. We should get that $\lambda_{n_u-n_p+1}$ is the first non-zero eigenvalue. Otherwise, spurious pressure modes are present in our finite element discretization.

Summarizing, to perform the inf-sup test it is necessary to design a proper analysis problem and consider a sequence of meshes to evaluate the first non-zero eigenvalue in eqn. (3.37). If the values obtained approach asymptotically a value greater than zero (and there are no spurious pressure modes) the inf-sup test is passed. Even though to pass the numerical inf-sup test does not guarantee that the inf-sup condition is satisfied in all cases, it is a very rigorous test. Results of the numerical inf-sup test applied to existing formulations can be seen in [1]. In chapter 4 we implement this test for our proposed element.

Chapter 4

Development of the element

In this chapter we present a new formulation which shows promise for general compressible and incompressible analysis of solids and fluids. First, we present our proposed element which is based on a mixed interpolation of displacements (velocities), pressure and strains (velocity strains). We implement the inf-sup test in section 4.2 and also discuss other possibilities that can be used in the selection of the interpolation fields in the last section.

4.1 The new proposed element

4.1.1 Variational formulation

Let \mathcal{B} be a general body in the space with prescribed displacements over the boundary S_u , applied tractions over S_f and $S_u \cap S_f = \emptyset$. The material response is assumed to be represented by a polyconvex stored energy function $W(\mathbf{x}, \boldsymbol{\epsilon})$, where \mathbf{x} indicates material points and $\boldsymbol{\epsilon}$ denotes the strain tensor. We can always split the strain tensor into a deviatoric and spherical or volumetric part,

$$\boldsymbol{\epsilon}' = \boldsymbol{\epsilon} - \frac{1}{3} \text{tr}(\boldsymbol{\epsilon}) \boldsymbol{\delta} ; \quad \text{tr}(\boldsymbol{\epsilon}') = 0 \quad (4.1)$$

$$\epsilon_v = \text{tr}(\boldsymbol{\epsilon}) \quad (4.2)$$

where $\boldsymbol{\delta}$ denotes the unit second order tensor.

The stress tensor and the constitutive tensor are given by

$$\boldsymbol{\tau} = \frac{\partial W(\mathbf{x}, \boldsymbol{\epsilon})}{\partial \boldsymbol{\epsilon}} \quad (4.3)$$

$$\mathbf{C} = \frac{\partial^2 W(\mathbf{x}, \boldsymbol{\epsilon})}{\partial \boldsymbol{\epsilon} \partial \boldsymbol{\epsilon}} \quad (4.4)$$

Note that the tensor \mathbf{C} as defined in (4.4) is neither isotropic nor constant. Moreover, it only depends on the stored energy function $W(\mathbf{x}, \boldsymbol{\epsilon})$.

We now assume a physical situation in which volumetric and deviatoric response are uncoupled and by virtue of the kinematic split (4.1) and (4.2) we can rewrite W as a function of $\boldsymbol{\epsilon}'$ and ϵ_v . Namely, $W(\mathbf{x}, \boldsymbol{\epsilon})$ can be written as

$$W(\mathbf{x}, \boldsymbol{\epsilon}) = W'(\mathbf{x}, \boldsymbol{\epsilon}') + W_v(\mathbf{x}, \epsilon_v) \quad (4.5)$$

and now

$$\boldsymbol{\tau}' = \frac{\partial W'(\mathbf{x}, \boldsymbol{\epsilon}')}{\partial \boldsymbol{\epsilon}'} \quad \mathbf{C}' = \frac{\partial^2 W'(\mathbf{x}, \boldsymbol{\epsilon}')}{\partial \boldsymbol{\epsilon}' \partial \boldsymbol{\epsilon}'} \quad (4.6)$$

$$p = \frac{\partial W_v(\mathbf{x}, \epsilon_v)}{\partial \epsilon_v} \quad \kappa = -\frac{\partial^2 W_v(\mathbf{x}, \epsilon_v)}{\partial \epsilon_v \partial \epsilon_v} \quad (4.7)$$

where $\boldsymbol{\tau}'$ is the deviatoric part of the stress tensor and p is the pressure. In the following we will refer to isotropic elasticity with constant material properties. We call \mathbf{C}' the stress-strain matrix law and κ the bulk modulus. However, because of the generality of the variational principles, our results are applicable to any solid provided the corresponding expression of the stored energy function is used. Moreover, they are also valid even if the material response cannot be uncoupled as assumed in eqn.

(4.5).

Let us consider the following variational indicator [1]

$$\Pi^*(\mathbf{u}, p) = \int_V \left[\frac{1}{2} \boldsymbol{\epsilon}' \cdot \mathbf{C}' \cdot \boldsymbol{\epsilon}' + \frac{1}{2} \frac{p^2}{\kappa} - p \left(\frac{p}{\kappa} + \epsilon_v \right) \right] dV - \mathcal{R}(\mathbf{u}) \quad (4.8)$$

where \mathbf{u} denotes the displacement field. The term $\mathcal{R}(\mathbf{u})$ accounts for the externally applied body forces \mathbf{f}^B and surface tractions \mathbf{f}^{Sf} ,

$$\mathcal{R}(\mathbf{u}) = \int_V \mathbf{u} \cdot \mathbf{f}^B dV + \int_{S_f} \mathbf{u}^{Sf} \cdot \mathbf{f}^{Sf} dS_f \quad (4.9)$$

Inspired by the developments given in [5] and [14], we write the strain field as,

$$\boldsymbol{\epsilon} = \partial_{\boldsymbol{\epsilon}} \mathbf{u} + \tilde{\boldsymbol{\epsilon}} \quad (4.10)$$

where $\partial_{\boldsymbol{\epsilon}} \mathbf{u}$ is the strain corresponding to the displacement field \mathbf{u} and $\tilde{\boldsymbol{\epsilon}}$ represents an enhancement in the strain field. The deviatoric and volumetric strains are now given by,

$$\boldsymbol{\epsilon}' = \partial_{\boldsymbol{\epsilon}'} \mathbf{u} + \tilde{\boldsymbol{\epsilon}}' \quad (4.11)$$

$$\epsilon_v = \partial_{\epsilon_v} u + \tilde{\epsilon}_v \quad (4.12)$$

Substituting from eqns. (4.11) and (4.12) into eqn. (4.8), we obtain

$$\begin{aligned} \tilde{\Pi}(\mathbf{u}, \tilde{\boldsymbol{\epsilon}}, p) = \int_V \left[\frac{1}{2} (\partial_{\boldsymbol{\epsilon}'} \mathbf{u} + \tilde{\boldsymbol{\epsilon}}') \cdot \mathbf{C}' \cdot (\partial_{\boldsymbol{\epsilon}'} \mathbf{u} + \tilde{\boldsymbol{\epsilon}}') - \right. \\ \left. \frac{1}{2} \frac{p^2}{\kappa} - p (\partial_{\epsilon_v} u + \tilde{\epsilon}_v) \right] dV - \mathcal{R}(\mathbf{u}) \end{aligned} \quad (4.13)$$

Note that we obtain the stress tensor $\boldsymbol{\tau}$ as

$$\boldsymbol{\tau} = \boldsymbol{\tau}' - p \boldsymbol{\delta} \quad (4.14)$$

where the deviatoric part is

$$\boldsymbol{\tau}' = \mathbf{C}' (\partial_{\epsilon'} \mathbf{u} + \tilde{\boldsymbol{\epsilon}}') \quad (4.15)$$

Invoking stationarity of $\tilde{\Pi}$ we obtain the following governing variational equations,

$$\begin{aligned} \int_V [\partial_{\epsilon'} \delta \mathbf{u} \cdot \mathbf{C}' \cdot (\partial_{\epsilon'} \mathbf{u} + \tilde{\boldsymbol{\epsilon}}') - \partial_{\epsilon_v} \delta u p] dV - \delta \mathcal{R}(\mathbf{u}) &= 0 \\ \int_V [\delta \tilde{\boldsymbol{\epsilon}}' \cdot \mathbf{C}' \cdot (\partial_{\epsilon'} \mathbf{u} + \tilde{\boldsymbol{\epsilon}}') - p \delta \tilde{\epsilon}_v] dV &= 0 \\ \int_V [-\delta p (\frac{p}{\kappa} + (\partial_{\epsilon_v} u + \tilde{\epsilon}_v))] dV &= 0 \end{aligned} \quad (4.16)$$

The first of eqns. (4.16) gives the well-known equilibrium equation and the last one gives the relation between pressure and volumetric strain. Since we know that the stress field cannot be zero under the action of externally applied loads the second equation imposes conditions to the enhanced strain field, which means that it cannot be arbitrarily selected. In fact, for the constant stress field case (patch test) the second of eqns. (4.16) becomes,

$$\boldsymbol{\tau} \cdot \int_V \delta \tilde{\boldsymbol{\epsilon}} dV = 0 \quad (4.17)$$

which means that the integral of the enhanced strain field must vanish. We will choose our finite element interpolations of the enhanced strain field such that condition (4.17) is satisfied and will refer to this point in more detail in the following section.

4.1.2 Implementation

The geometry and the displacement field are described using the standard 4-node isoparametric interpolations

$$\mathbf{x} = \sum_{i=1}^4 h_i(\mathbf{r}) \mathbf{x}_i \quad (4.18)$$

$$\mathbf{u} = \sum_{i=1}^4 h_i(\mathbf{r}) \mathbf{u}_i \quad (4.19)$$

In these equations, h_i are the usual interpolation functions, \mathbf{r} indicates the isoparametric coordinates, and \mathbf{x}_i and \mathbf{u}_i are the nodal point coordinates and nodal point displacements, respectively. The deviatoric and volumetric strains corresponding to \mathbf{u} are

$$\partial_{e'} \mathbf{u} = \mathbf{B}'(\mathbf{r}) \hat{\mathbf{u}} \quad (4.20)$$

$$\partial_{e_v} u = \mathbf{B}_v(\mathbf{r}) \hat{\mathbf{u}} \quad (4.21)$$

where $\mathbf{B}'(\mathbf{r})$ and $\mathbf{B}_v(\mathbf{r})$ are, respectively, the corresponding strain interpolation matrices and $\hat{\mathbf{u}}$ contains the nodal point displacements.

The crucial ingredients of the element formulation are the interpolations of the pressure field and the enhanced strain field. As is well known, using the bilinear displacement interpolation and no enhanced strain field (that is, using $\tilde{\boldsymbol{\epsilon}} = \mathbf{0}$), the “best” element is the displacement/constant pressure element (the 4/1 or Q1/P0 element). Any higher order pressure interpolation deteriorates the element performance in almost incompressible analysis, and even the constant pressure element is not reliable (unless used in certain macro-element patterns). The 4/1 element does not satisfy the inf-sup condition.

We are using the enhancement in the strain field to increase the predictive capa-

bility of the element in bending and enlarge at the same time the “divergence space” of the element. Based on these thoughts, we propose to use the same interpolation for the pressure as for the displacements, that is

$$p = \sum_{i=1}^4 h_i(\mathbf{r}) p_i = \mathbf{H}(\mathbf{r}) \hat{\mathbf{p}} \quad (4.22)$$

where the p_i are the nodal point pressure values.

Hence the element will yield a continuous pressure field across the element boundaries.

With the above displacement and pressure interpolations it is now crucial to select an appropriate strain field $\tilde{\boldsymbol{\epsilon}}$.

Let us define the enhanced strain field interpolation as

$$\tilde{\boldsymbol{\epsilon}} = \mathbf{G}(\mathbf{r}) \boldsymbol{\alpha} \quad (4.23)$$

The matrix $\mathbf{G}(\mathbf{r})$ (to be defined in detail) contains functions of \mathbf{r} and the vector $\boldsymbol{\alpha}$ contains the internal element parameters.

Using eqns. (4.18) to (4.23) in eqns. (4.16) we obtain the following discrete finite element equations,

$$\begin{bmatrix} \mathbf{K}_{uu} & \mathbf{K}_{u\alpha} & \mathbf{K}_{up} \\ \mathbf{K}_{u\alpha}^T & \mathbf{K}_{\alpha\alpha} & \mathbf{K}_{\alpha p} \\ \mathbf{K}_{up}^T & \mathbf{K}_{\alpha p}^T & \mathbf{K}_{pp} \end{bmatrix} \begin{Bmatrix} \hat{\mathbf{u}} \\ \boldsymbol{\alpha} \\ \hat{\mathbf{p}} \end{Bmatrix} = \begin{Bmatrix} \mathbf{R} \\ \mathbf{0} \\ \mathbf{0} \end{Bmatrix} \quad (4.24)$$

where

$$\begin{aligned}
\mathbf{K}_{uu} &= \int_V \mathbf{B}'^T(\mathbf{r}) \mathbf{C}' \mathbf{B}'(\mathbf{r}) \, dV & \mathbf{K}_{up} &= - \int_V \mathbf{B}'^T(\mathbf{r}) \mathbf{H}(\mathbf{r}) \, dV \\
\mathbf{K}_{pp} &= - \int_V \frac{1}{\kappa} \mathbf{H}^T(\mathbf{r}) \mathbf{H}(\mathbf{r}) \, dV & \mathbf{K}_{\alpha p} &= - \int_V \mathbf{G}'^T(\mathbf{r}) \mathbf{H}(\mathbf{r}) \, dV \\
\mathbf{K}_{\alpha\alpha} &= \int_V \mathbf{G}'^T(\mathbf{r}) \mathbf{C}' \mathbf{G}'(\mathbf{r}) \, dV & \mathbf{K}_{u\alpha} &= \int_V \mathbf{B}'^T(\mathbf{r}) \mathbf{C}' \mathbf{G}'(\mathbf{r}) \, dV
\end{aligned} \tag{4.25}$$

and \mathbf{R} is the usual load vector.

The final stiffness matrix is obtained by statically condensing out the internal parameters $\boldsymbol{\alpha}$ at the element level.

The matrix $\mathbf{G}(\mathbf{r})$ must satisfy the requirement that the linear system of equations (4.24) be solvable, that is, after elimination of the physical rigid body modes. We also want that the element passes the patch test.

Of course, satisfying these requirements does not assure that we have a stable finite element discretization. However, this solvability condition is necessary and the passing of the patch test indicates whether the element will be useful. Ideally, as mentioned above, we would be able to analytically show that the element formulation satisfies the inf-sup condition for incompressible analysis.

The system of equations (4.24) will be solvable if the matrix $\mathbf{K}_{\alpha\alpha}$ is invertible, which is guaranteed if the columns of the matrix $\mathbf{G}(\mathbf{r})$ are linearly independent. According to our variational principle, the integral of $\tilde{\epsilon}$ over the volume of the element must vanish. Hence, assuming a constant thickness we must have

$$\int_{-1}^{+1} \int_{-1}^{+1} \mathbf{G}(\mathbf{r}) \, J(\mathbf{r}) \, d\mathbf{r} = \mathbf{0} \tag{4.26}$$

where $J(\mathbf{r})$ is the Jacobian determinant for the transformation from the physical

coordinates (x,y) to the isoparametric coordinates (r,s) .

We will now establish the enhanced strain interpolation defined in eqn. (4.23). Let us consider first a square element of size 2×2 . In this case we use $\mathbf{G}(\mathbf{r}) = \mathbf{G}^*(\mathbf{r})$,

$$\mathbf{G}^*(\mathbf{r}) = \begin{bmatrix} r & 0 & 0 & 0 & rs & 0 \\ 0 & s & 0 & 0 & 0 & rs \\ 0 & 0 & r & s & 0 & 0 \end{bmatrix} \quad (4.27)$$

Note that the first four columns of \mathbf{G}^* define the strain interpolations that actually correspond to the incompatible displacement interpolations used in the element of Wilson [14]. The two columns that we add in $\mathbf{G}^*(\mathbf{r})$ enable the element to pass the numerical inf-sup test given in section 3.3.

If the element is a general quadrilateral we need to transform the strains in the isoparametric coordinate system to the physical coordinate system and we perform this tensor transformation in matrix form,

$$\mathbf{G}(\mathbf{r}) = \frac{J_0}{J(\mathbf{r})} \bar{\mathbf{X}}_0 \mathbf{G}^*(\mathbf{r}) \quad (4.28)$$

where

$$\bar{\mathbf{X}}_0^{-1} = \begin{bmatrix} X_{011}^2 & X_{021}^2 & X_{011}X_{021} \\ X_{012}^2 & X_{022}^2 & X_{012}X_{022} \\ 2X_{012}X_{011} & 2X_{021}X_{022} & X_{011}X_{022} + X_{012}X_{021} \end{bmatrix} \quad (4.29)$$

and

$$\mathbf{X}_0 = \left. \frac{\partial \mathbf{x}(\mathbf{r})}{\partial \mathbf{r}} \right|_{\mathbf{r}=\mathbf{0}}; \quad \text{and} \quad J_0 = J|_{\mathbf{r}=\mathbf{0}} \quad (4.30)$$

Hence, we use in eqn. (4.28) the geometry gradient and determinant evaluated at the center of the element. Since the condition (4.26) is satisfied for the square element,

the same condition is also satisfied for the element of general geometric shape.

We note that, of course, higher order terms can be included in the strain interpolation matrix $\mathbf{G}^*(\mathbf{r})$ provided condition (4.26) is satisfied. However, we performed some numerical experimentation which showed that no significant improvements are obtained by including higher-order terms (see section 4.3).

4.1.3 The axisymmetric element

For axisymmetric analysis due to the hoop strain and the presence of the factor $x_r(\mathbf{r})$ (the radius expressed as a function of the natural coordinates) in the integrations, some extensions of the above element formulation are needed.

To include an enhancement for the hoop strain we modify the enhanced strain interpolation (4.27). Consider the 2x2 element and the interpolation matrix

$$\tilde{\mathbf{G}}^*(\mathbf{r}) = \begin{bmatrix} r & 0 & 0 & 0 & rs & 0 \\ 0 & s & 0 & 0 & 0 & rs \\ 0 & 0 & r & s & 0 & 0 \\ 0 & 0 & 0 & 0 & rs & rs \end{bmatrix} \quad (4.31)$$

Using $\tilde{\mathbf{G}}^*(\mathbf{r})$ condition (4.26) is now violated due to the additional thickness factor $x_r(\mathbf{r})$ in the integral and a normalization of the interpolation (4.31) is required.

Let

$$\mathbf{G}^*(\mathbf{r}) = \tilde{\mathbf{G}}^*(\mathbf{r}) + \tilde{\mathbf{G}}_c^* \quad (4.32)$$

where $\tilde{\mathbf{G}}_c^*$ is a correction matrix of constant elements to satisfy eqn. (4.26). Then we obtain

$$\mathbf{G}^*(\mathbf{r}) = \tilde{\mathbf{G}}^*(\mathbf{r}) - \frac{1}{\int_{-1}^1 \int_{-1}^1 x_r(\mathbf{r}) d\mathbf{r}} \int_{-1}^1 \int_{-1}^1 \tilde{\mathbf{G}}^*(\mathbf{r}) x_r(\mathbf{r}) d\mathbf{r} \quad (4.33)$$

The matrix $\mathbf{G}(\mathbf{r})$ for a general quadrilateral element is then obtained by the transformations defined in eqns. (4.28) to (4.30).

4.2 Implementation of the numerical inf-sup test

In the numerical inf-sup test we choose an analysis problem and investigate whether the inf-sup values in the finite element solutions of that problem, with increasingly finer meshes, are bounded. We choose the constrained cavity and the cantilever problem shown in Figure 4-1 to perform our analysis.

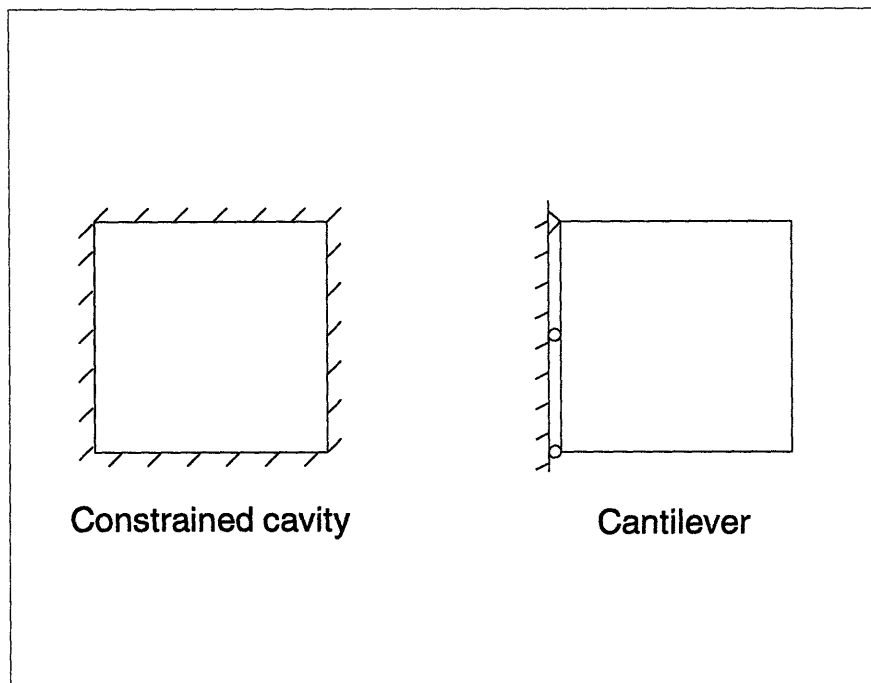


Figure 4-1: Inf-sup test. Problems considered

We use here the inf-sup condition as written in terms of the nodal quantities (eqn. (3.34)) and solve the eigenproblem given by eqn. (3.37).

The key is the evaluation of the matrices \mathbf{G}_h and \mathbf{S}_h defined by eqns. (3.35) and (3.36) respectively. To this end we consider the matrix problem that corresponds to

the variational formulation defined in eqns. (4.16),

$$\begin{bmatrix} \mathbf{A}_h & \mathbf{B}_h^T \\ \mathbf{B}_h & -\frac{1}{\kappa} \mathbf{T}_h \end{bmatrix} \begin{Bmatrix} \tilde{\mathbf{U}}_h \\ \mathbf{P}_h \end{Bmatrix} = \begin{Bmatrix} \tilde{\mathbf{F}}_h \\ \mathbf{0} \end{Bmatrix} \quad (4.34)$$

From eqn. (4.24) we can immediately identify,

$$\mathbf{A}_h = \begin{bmatrix} (\mathbf{K}_{uu})_h & (\mathbf{K}_{u\alpha})_h \\ (\mathbf{K}_{u\alpha})_h^T & (\mathbf{K}_{\alpha\alpha})_h \end{bmatrix} \quad (4.35)$$

$$\mathbf{B}_h^T = \begin{bmatrix} (\mathbf{K}_{up})_h \\ (\mathbf{K}_{\alpha p})_h \end{bmatrix} \quad (4.36)$$

$$\mathbf{T}_h = \int_V \mathbf{H}^T(\mathbf{r}) \mathbf{H}(\mathbf{r}) dV \quad (4.37)$$

$$\tilde{\mathbf{U}}_h = \begin{Bmatrix} \hat{\mathbf{u}} \\ \boldsymbol{\alpha} \end{Bmatrix} \quad (4.38)$$

$$\mathbf{P}_h = \{\hat{\mathbf{p}}\} \quad (4.39)$$

$$\tilde{\mathbf{F}}_h = \begin{Bmatrix} \mathbf{R}(\mathbf{u}) \\ \mathbf{0} \end{Bmatrix} \quad (4.40)$$

\mathbf{G}_h is now directly obtained from, [11]

$$\mathbf{G}_h = \mathbf{B}_h^T \mathbf{T}_h^{-1} \mathbf{B}_h \quad (4.41)$$

Note that externally applied loads and material parameters do not affect the expressions in eqns. (3.35) to (3.37).

The evaluation of \mathbf{S}_h must include the fact that we are interpolating not only the displacements but also strains. Making use of Korn's inequality [17], we therefore use instead of the 1-norm that enters in eqn. (3.26) and evaluated in eqn. (3.35), an equivalent norm defined in terms of the components of the strain tensor,

$$|\mathbf{v}| = \left(\sum_{i,j=1}^3 \|\epsilon_{ij}\|^2 \right)^{1/2} \quad (4.42)$$

Figure 4-2 shows the results of the test applied to the constrained cavity shown in Figure 4-1. The figure shows that the test is passed. Also, the count of the number of zero eigenvalues, after removal of the physical pressure mode, shows that spurious modes are not present.

The evaluation of the inf-sup value was performed for three uniform meshes in which $N=2,4,8$ where N is equal to the number of elements per side. $IS = \sqrt{\lambda_p}$, where λ_p is the smallest nonzero eigenvalue.

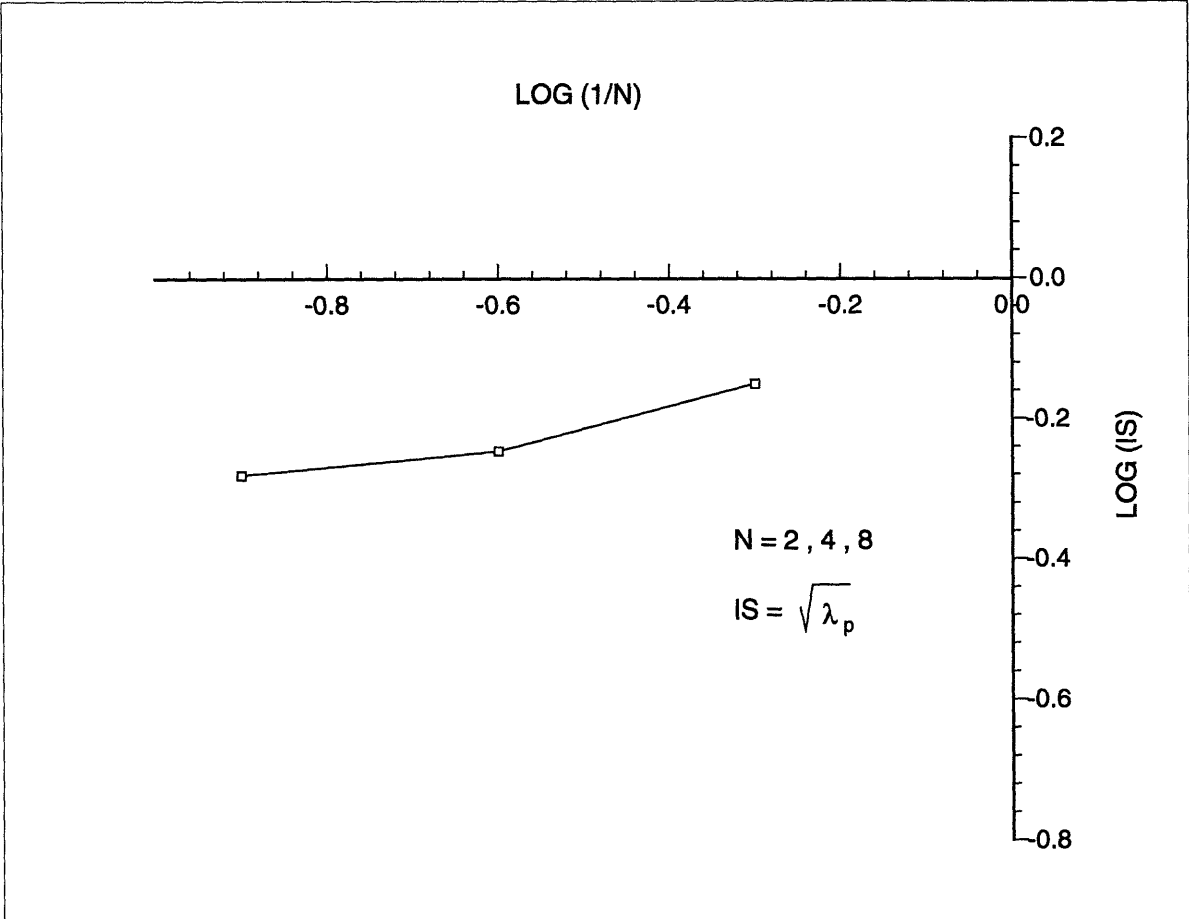


Figure 4-2: Results of the inf-sup test for the constrained cavity shown in Figure 4.1. N is the number of elements per side of plate in Figure 4.1 and IS is the calculated inf-sup value

The results of the numerical inf-sup test applied to the cantilever problem shown in Figure 4-1 are shown in Figure 4-3. We performed the test over a regular and a distorted mesh. The test is passed in both cases. It can be inferred from the picture that the distortion of the elements does not affect appreciably the results.

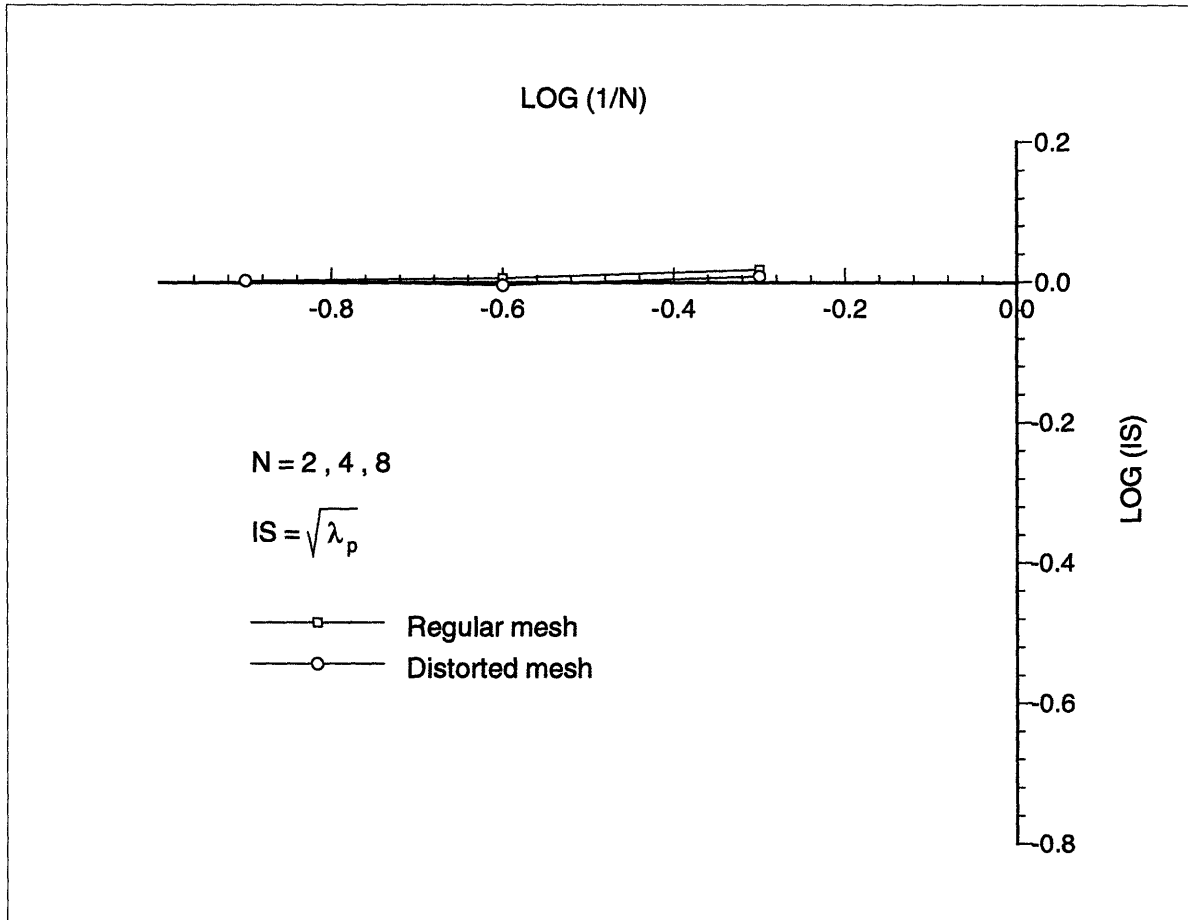


Figure 4-3: Results of the inf-sup test for the cantilever problem shown in Figure 4.1. N is the number of elements per side of plate in Figure 4.1 and IS is the calculated inf-sup value

4.3 Other possibilities in the selection of interpolation fields

Since we are interpolating both, the strain and pressure fields, many possibilities are open to select their approximations. Of course, once we choose the interpolations we

do not know a priori whether they will work or not. However, based on theoretical knowledge we can predict if a certain selection will fail or not. Other cases are not so obvious and their usefulness is determined by numerical experience.

We want to discuss in this section different approaches that we have investigated and the thoughts that guided us to arrive to our final results.

The main objective is to develop a new element that satisfies the relevant inf-sup condition. The numerical inf-sup test presented in chapter 3 and implemented in section 4.2 when strain interpolations are used, is employed as a tool to predict whether the element is likely to satisfy the inf-sup condition. Ideally a mathematical proof is available.

To establish the approximations for our element, we focus our attention on some well-known elements like the 4/1, 4/3, 9/3 and 9/4-c elements. These elements fall in the context of the u/p formulation and analytical proofs that determine whether they satisfy the inf-sup condition are available [1],[10]. The first two do not satisfy the inf-sup condition. The 4/1 element presents spurious pressure modes under certain modeling conditions while in the 4/3 element the pressure space is too large to satisfy the incompressibility constraint. On the other hand, for the last two, the inf-sup condition is satisfied. Also, nine-node elements present an additional advantage, namely, they give exact results under bending action even if distorted elements are used.

4.3.1 The enhanced strain field interpolation

Since it is the strain field that enters in the potential Π defined in eqn. (4.8), we begin our analysis by comparing the strain field obtained with the four-node and the nine-node square elements (note that the Jacobian matrix is constant in this case). Let us first construct the \mathbf{B} matrix for the four-node square element. By inspection, we determine that it spans the same space as the column space of the following linear operator

$$\mathbf{B}_1(\mathbf{r}) = \begin{bmatrix} 1 & 0 & 0 & s & 0 & 0 & 0 \\ 0 & 1 & 0 & 0 & r & 0 & 0 \\ 0 & 0 & 1 & 0 & 0 & r & s \end{bmatrix} \quad (4.43)$$

We now consider the space generated by the \mathbf{B} matrix obtained from the nine-node displacement interpolations. To obtain this space, it is necessary to add the following columns to \mathbf{B}_1

$$\mathbf{G}_1(\mathbf{r}) = \begin{bmatrix} r & 0 & rs & 0 & 0 & s^2 & 0 & 0 & 0 & rs^2 & 0 & 0 & 0 \\ 0 & s & 0 & rs & 0 & 0 & r^2 & 0 & 0 & 0 & sr^2 & 0 & 0 \\ 0 & 0 & 0 & 0 & rs & 0 & 0 & r^2 & s^2 & 0 & 0 & sr^2 & rs^2 \end{bmatrix} \quad (4.44)$$

We remark that in the case of distorted elements the Jacobian matrix is no longer constant and the above matrix entries are changed.

Let us now concentrate on expression (4.44). We could use \mathbf{G}_1 as our enhanced strain field interpolation (eqn. (4.27)). However, we can immediately appreciate that \mathbf{G}_1 does not satisfy condition (4.26) which implies that the patch test will not be passed. Clearly, the integral over the volume of the element of terms like r^2 and s^2 is not zero. Deleting the columns in \mathbf{G}_1 that contain those terms will leave us with condition (4.26) satisfied at the price of losing the capabilities of the nine-node element. Therefore, we have

$$\mathbf{G}'(\mathbf{r}) = \begin{bmatrix} r & 0 & rs & 0 & 0 & rs^2 & 0 & 0 & 0 \\ 0 & s & 0 & rs & 0 & 0 & sr^2 & 0 & 0 \\ 0 & 0 & 0 & 0 & rs & 0 & 0 & sr^2 & rs^2 \end{bmatrix} \quad (4.45)$$

Using this operator as our enhanced strain interpolations requires the inversion of a 9x9 matrix to condense out the internal parameters α . Furthermore, exact integration requires the use of a 3x3 quadrature rule which would make the element very expensive. The computational cost can be reduced further by noting that numerical results are not much affected if we neglect the last four columns in (4.45). However, the resulting enhanced strain interpolation operator still differs from the one that we have defined in (4.27). Our numerical experience showed that better results are obtained if we use (4.27) when distorted elements are present in the model. Thus, we finally use,

$$\mathbf{G}^*(\mathbf{r}) = \begin{bmatrix} r & 0 & 0 & 0 & rs & 0 \\ 0 & s & 0 & 0 & 0 & rs \\ 0 & 0 & r & s & 0 & 0 \end{bmatrix} \quad (4.46)$$

If the last two columns of \mathbf{G}^* are not used the incompatible element of Wilson [14] is recovered. We would like to make some comments at this point regarding the use of

$$\mathbf{G}_w^*(\mathbf{r}) = \begin{bmatrix} r & 0 & 0 & 0 \\ 0 & s & 0 & 0 \\ 0 & 0 & r & s \end{bmatrix} \quad (4.47)$$

First of all, the patch test is passed since \mathbf{G}_w^* satisfies condition (4.26). Let us now consider the cantilever problem that we use in Section 4.2 to perform the numerical inf-sup test. We clearly have in this model, if we use (4.47), that $n_u \geq n_p$ which is a necessary condition for a discretization to be stable but not sufficient. In fact, the numerical inf-sup test is not passed. A spurious pressure mode is present and the value of the first non-zero eigenvalue is not bounded from below as shown in Figure 4-4.

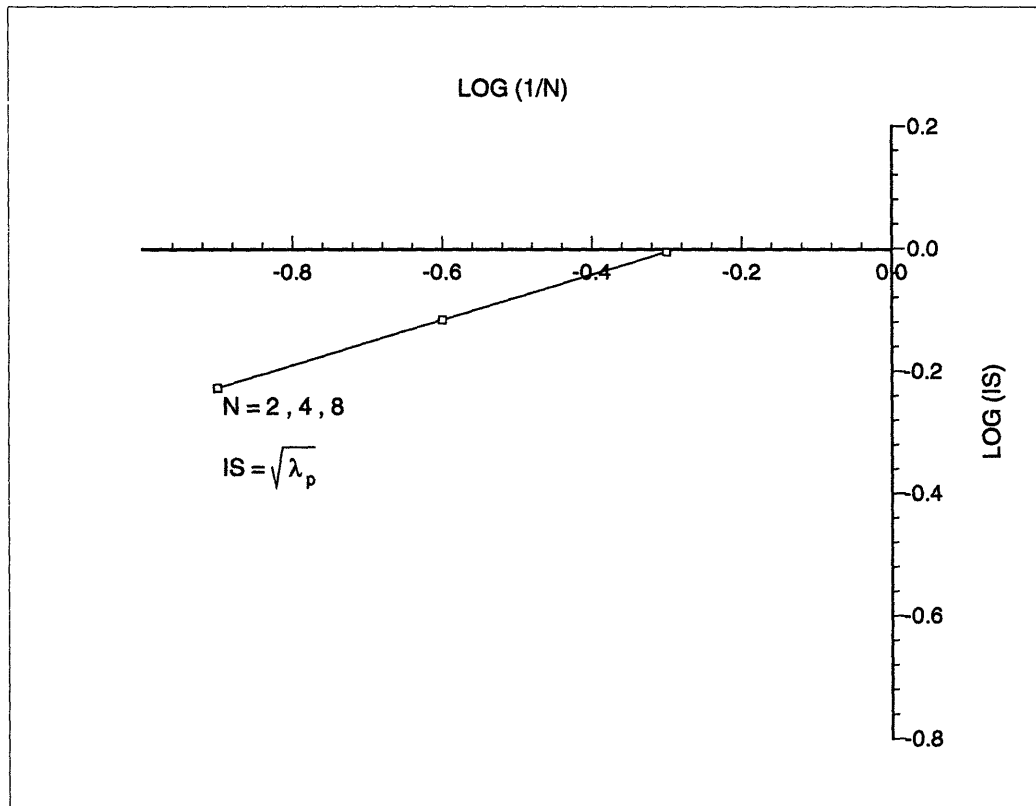


Figure 4-4: Results of the inf-sup test using the strain interpolations defined in eqn. (4.47). N is the number of elements per side of plate in Figure 4.1 and IS is the calculated inf-sup value

4.3.2 Pressure interpolations. Internal degrees of freedom

Once the strain interpolation functions have been defined, it only remains to decide the interpolation of the pressure field. We analyze in this section different options that can be considered.

Constant pressure interpolation

The pressure is defined to be constant throughout the element and the space Q_h defined in chapter 3 is the space of constant functions. In the context of the u/p formulation the equivalent element is the 4/1 or Q1-P0 element. We know that the 4/1 element has a spurious pressure mode. However, due to the fact that we have an

enhancement in the strain interpolations, we may expect that the spurious pressure modes be filtered out in the model.

Let us define now the following operators,

$$\mathbf{I}' = \mathbf{I} - \frac{1}{3} \boldsymbol{\delta} \otimes \boldsymbol{\delta} \quad (4.48)$$

$$\mathbf{I}_v = \frac{1}{3} \boldsymbol{\delta} \otimes \boldsymbol{\delta} \quad (4.49)$$

where \mathbf{I} is the unit fourth-order tensor with components $I_{ijkl} = \frac{1}{2} \{ \delta_{ik} \delta_{jl} + \delta_{il} \delta_{jk} \}$. They are linear operators that map a second order tensor into its deviatoric and spherical part respectively. Thus, we can apply these operators to each column of our enhanced strain operator (note that each column of \mathbf{G}^* is a second order tensor by itself) to obtain \mathbf{G}' and \mathbf{G}_v .

Clearly, the resulting operators \mathbf{G}' and \mathbf{G}_v will both satisfy similar conditions to (4.26), namely,

$$\int_{-1}^{+1} \int_{-1}^{+1} \mathbf{G}'(\mathbf{r}) \mathbf{J}(\mathbf{r}) \, d\mathbf{r} = \mathbf{0} \quad (4.50)$$

$$\int_{-1}^{+1} \int_{-1}^{+1} \mathbf{G}_v(\mathbf{r}) \mathbf{J}(\mathbf{r}) \, d\mathbf{r} = \mathbf{0} \quad (4.51)$$

Although we have enhanced the strain field, we will show that, as for the 4/1 element, a spurious pressure mode will appear in certain situations and the inf-sup condition is not satisfied. To demonstrate that a spurious pressure mode is present we need to prove that given a (non-zero) pressure distribution p we have

$$\int_{\Omega} p \, \text{div} \, \mathbf{v}_h \, d\Omega = 0 \quad \forall \mathbf{v}_h \in V_h \quad (4.52)$$

Let us consider a finite element discretization like the one shown in Figure 4-5 with the pressure distribution (checkerboard) indicated in Figure 4-6. In this model

all displacements along the boundary are set to zero.

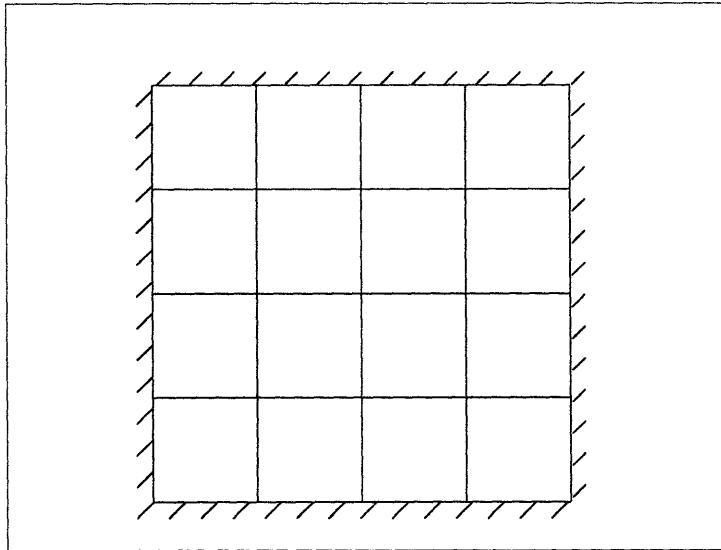


Figure 4-5: Spurious pressure modes. Element discretization

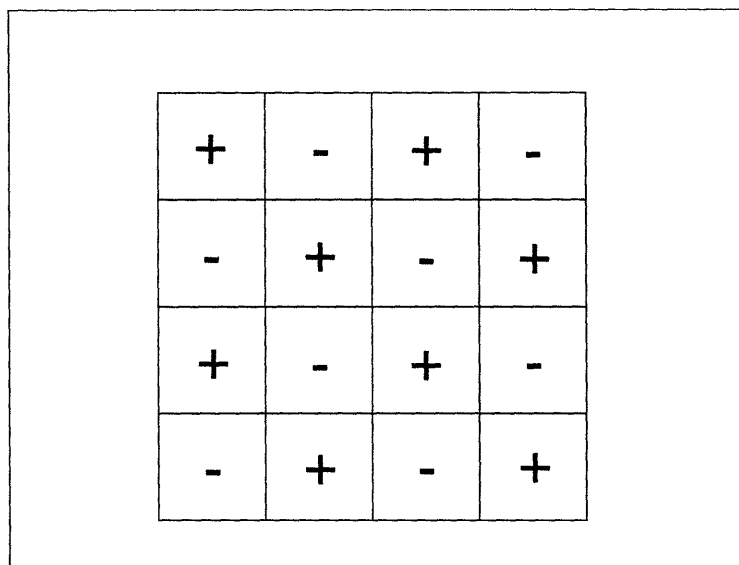


Figure 4-6: Spurious pressure modes. Checkerboard distribution

Over each element we have

$$\operatorname{div} \mathbf{u}_h = \epsilon_v = \partial_{\epsilon_v} u + \tilde{\epsilon}_v \quad (4.53)$$

where

$$\tilde{\epsilon}_v = \mathbf{G}_v \boldsymbol{\alpha} \quad (4.54)$$

and

$$\begin{aligned} \int_{\Omega_e} p_e \operatorname{div} \mathbf{u}_h d\Omega_e &= p_e \int_{\Omega_e} (\partial_{\epsilon_v} u + \tilde{\epsilon}_v) d\Omega_e && \text{use (4.53)} \\ &= p_e \int_{\Omega_e} (\partial_{\epsilon_v} u + \mathbf{G}_v \boldsymbol{\alpha}) d\Omega_e && \text{use (4.54)} \\ &= p_e \int_{\Omega_e} \partial_{\epsilon_v} u d\Omega_e && \text{use (4.51)} \end{aligned} \quad (4.55)$$

If a patch of four elements is considered, for the displacement u_i shown in Figure 4-7 we have,

$$\int_{\Omega} p \operatorname{div} \mathbf{u}_h d\Omega = [p^{e_1}(1) + p^{e_2}(-1) + p^{e_3}(1) + p^{e_4}(-1)] u_i = 0 \quad (4.56)$$

The same holds true when any displacement v_i is considered. Therefore, the relation (4.52) is satisfied for any nodal point displacement when the pressure distribution is the indicated checkerboard pressure.

We conclude that when using strain interpolations with the pressure field constant over the element the satisfaction of the inf-sup condition is not possible.

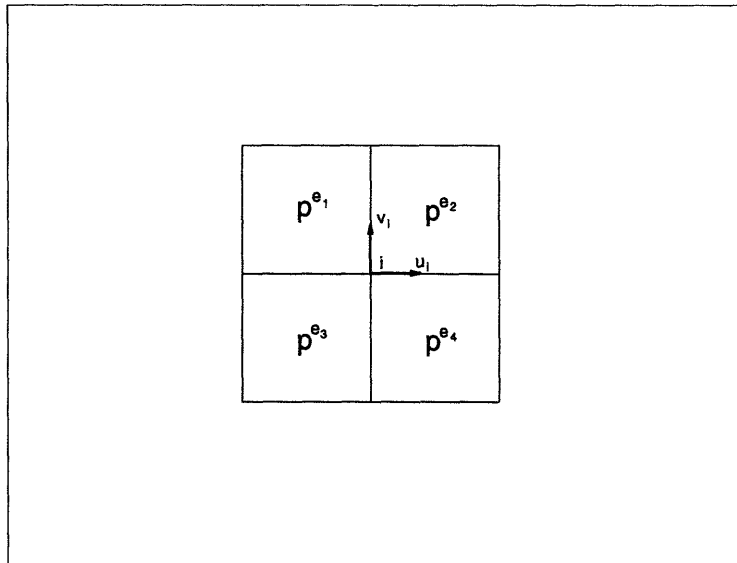


Figure 4-7: Spurious pressure modes. Patch of four equal elements

Linear pressure interpolation

We now discuss the possibility of using a linear pressure interpolation with internal degrees of freedom, that means, they can be condensed out at the element level. The pressure interpolation in this case is given by

$$p = \beta_1 + \beta_2 r + \beta_3 s \quad (4.57)$$

The space Q_h is defined as

$$Q_h = \{1, r, s\} \quad (4.58)$$

We can immediately see that, according to what we have discussed for the constant pressure interpolation, the first column of $\mathbf{K}_{\alpha p}$ is zero. The other two columns are different from zero and they add some extra terms that contribute to improve

the performance of the element with respect to the classical 4/3 element. However, pressure oscillations still exist in some cases (for example, driven cavity test) and we consider that the element is not reliable.

4.3.3 The use of bubble functions

The so-called *bubble functions* are used to enrich the displacement space. They consist of quadratic functions which vanish along the boundary of the element. The most common is the following function

$$h_b = (1 - r^2)(1 - s^2) \quad (4.59)$$

The added degrees of freedom are internal ones and can be condensed out at the element level. Since the bubble function values vanish along the boundary of the element, we end up with a compatible element.

Although we are introducing external degrees of freedom, it has been shown that the use of the bubble function presents no improvements in typical problems (see [20]). If a bubble function is used in the context of the u/p formulation, since its divergence has zero mean value, we can make a similar analysis as in section 4.3.2 to demonstrate that the inf-sup condition will not be satisfied.

Chapter 5

Numerical Tests

5.1 Beam Bending

A beam clamped at one end and subjected to an applied moment at the other end is modeled using two finite elements. The mesh is distorted by rotating the common edge of the elements. This is a classical test to evaluate the capabilities of elements when subjected to distortions. Figure 5-1 shows the calculated results in comparison with the analytical solution as a function of the degree of skew.

5.2 No-Flow test

An almost incompressible solid/fluid rests in a non-square cavity subjected to gravity loading, see Figure 5-2. The velocities normal to the walls are prescribed to be zero and the pressure at the free surface is $p = 0$. The solution must give zero displacements/velocities and a linear distribution in pressure. Our numerical results give negligible displacements/velocities (because we are using an almost incompressible material) and an almost linear distribution in pressure as shown in the figure. The deviation from linearity is larger when distorted elements are used.

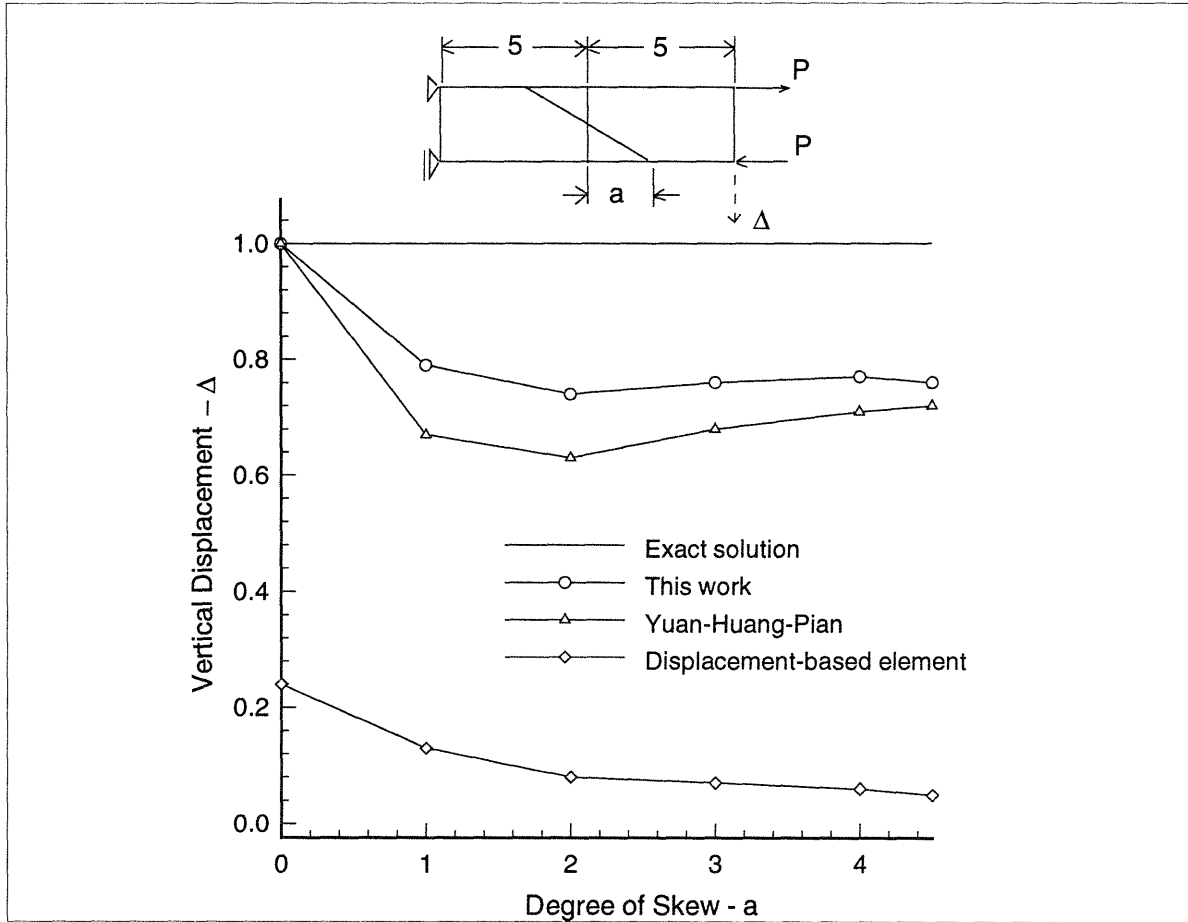


Figure 5-1: Bending test. Poisson's ratio = 0

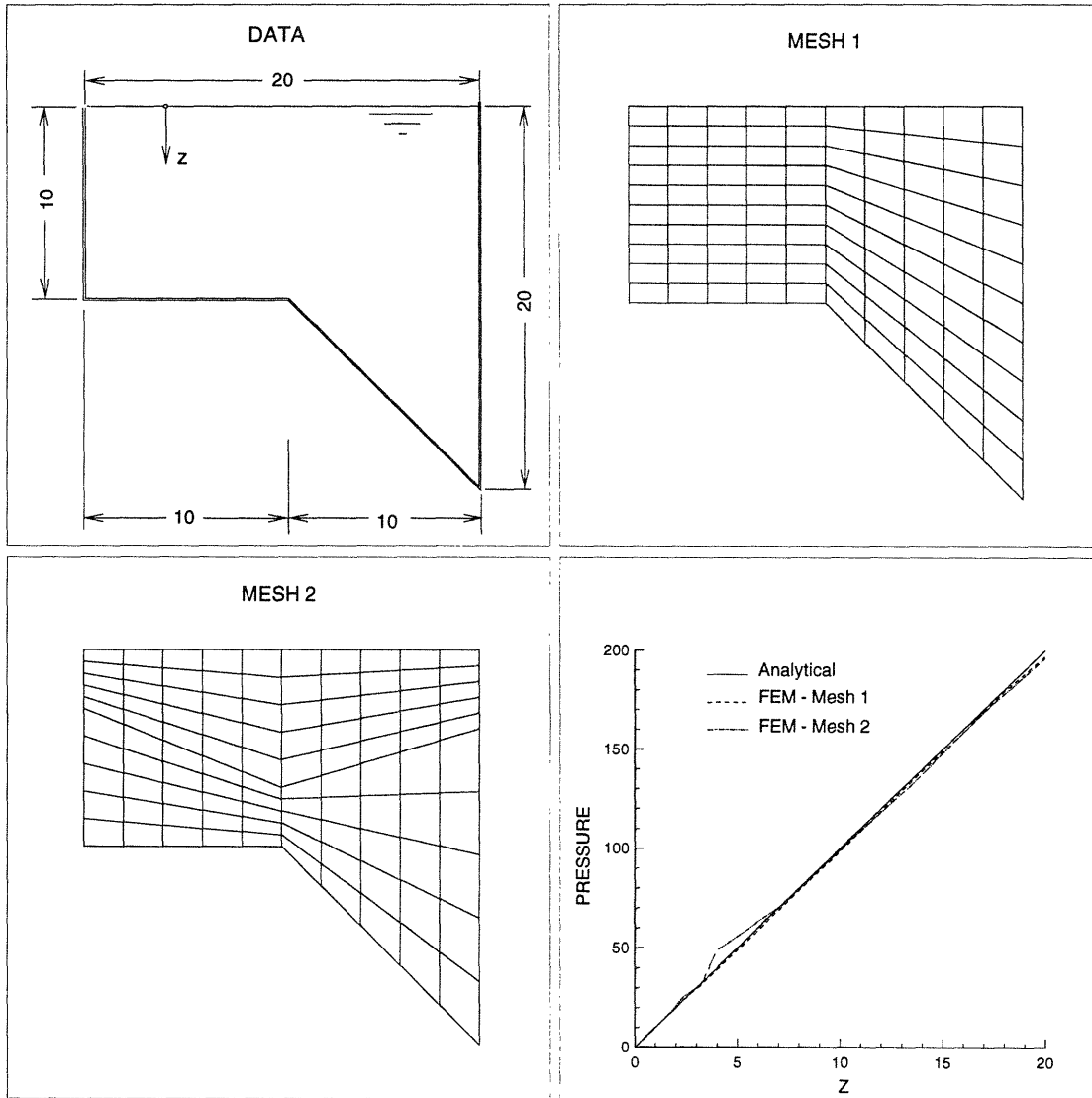


Figure 5-2: No-flow test

5.3 Driven Cavity

A square cavity with boundary velocities constrained to zero along three edges and a uniform prescribed velocity applied along the top edge is considered, see Figure

5-3. The pressure distribution compared with the 9/4-c (or Q2/Q1) element (that is, the biquadratic velocity and bilinear continuous pressure element) as well as pressure band plots are shown in Figure 5-4 for 10x10 and 20x20 meshes, respectively.

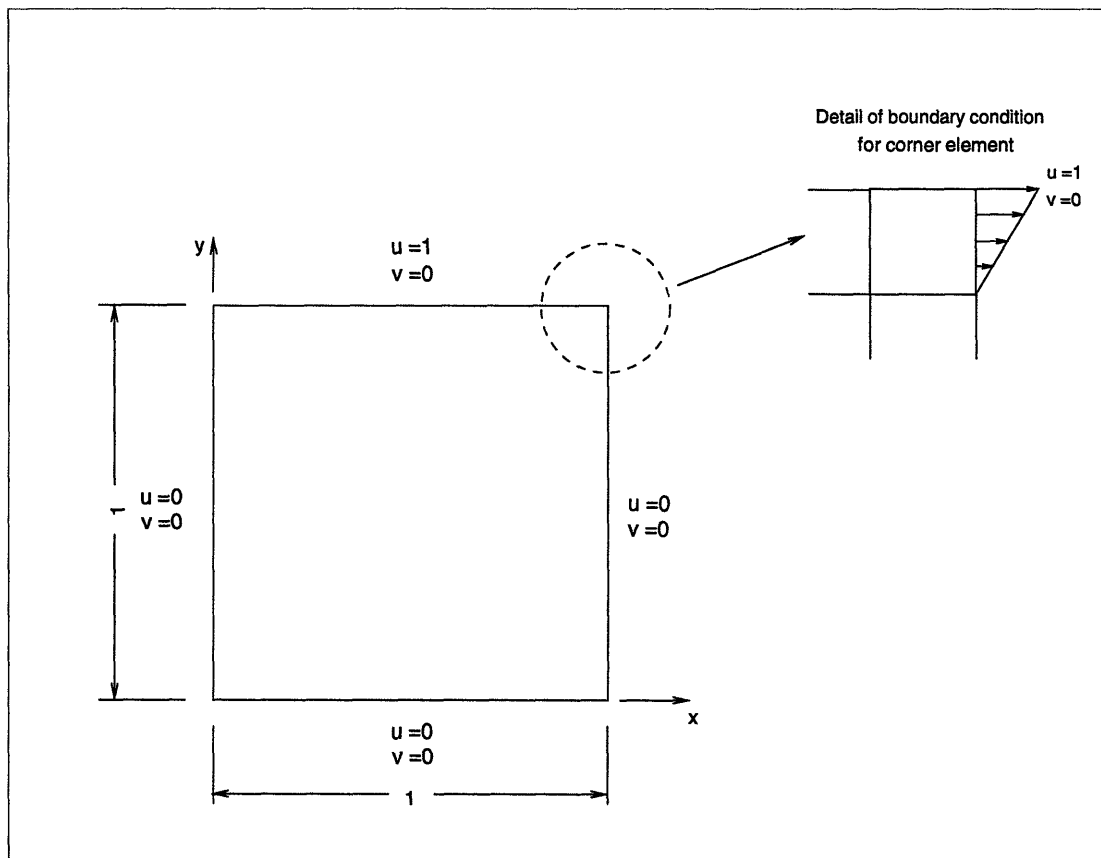


Figure 5-3: Driven cavity. Boundary condition at corner element

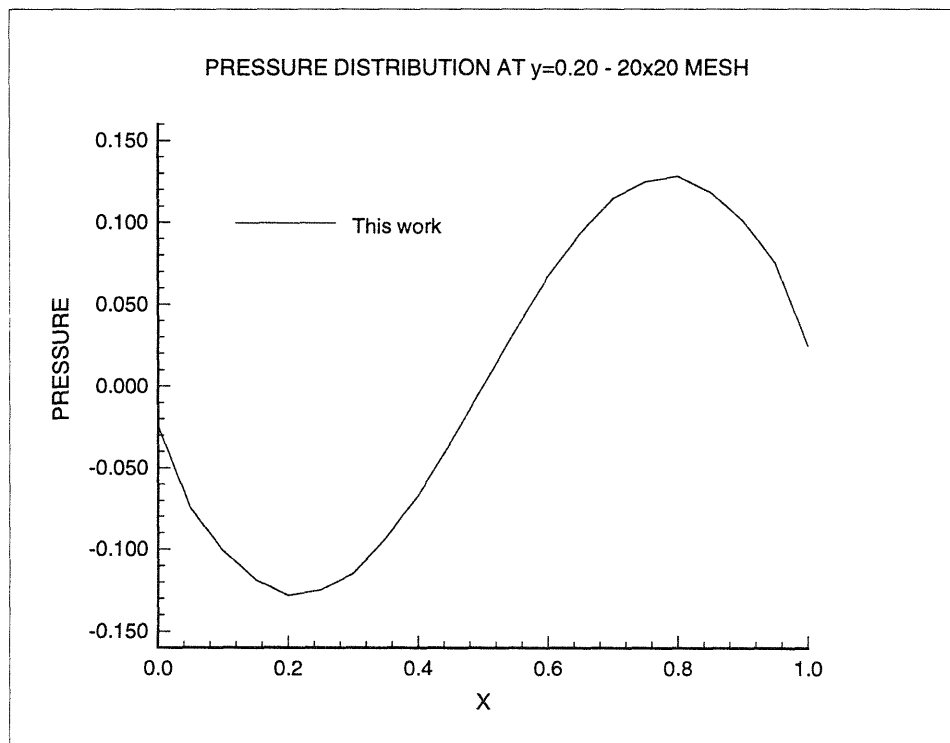
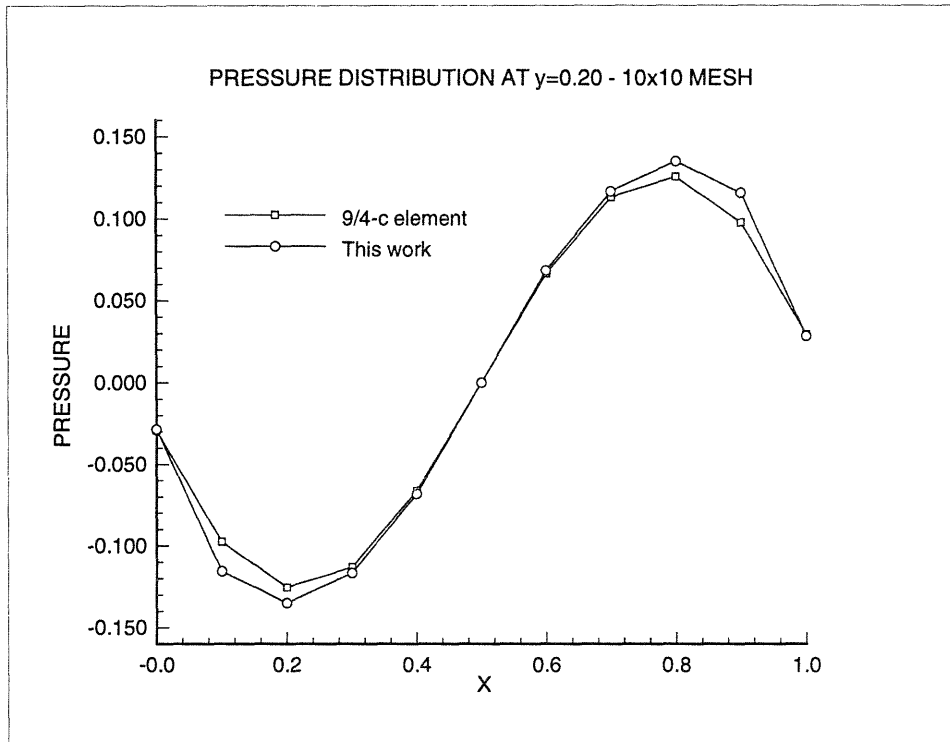


Figure 5-4: Driven cavity. Pressure distribution

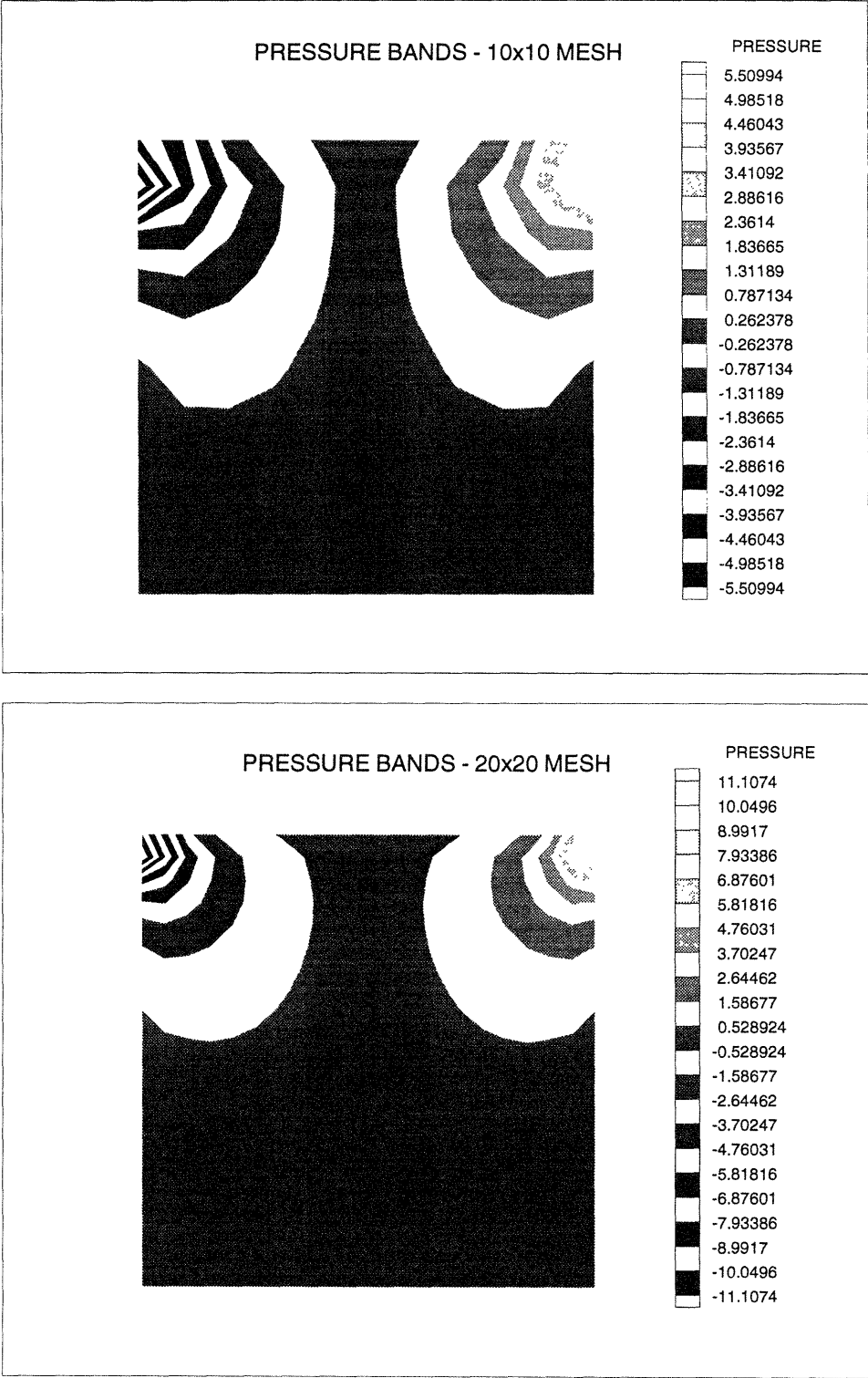


Figure 5-4: Driven cavity. Pressure bands

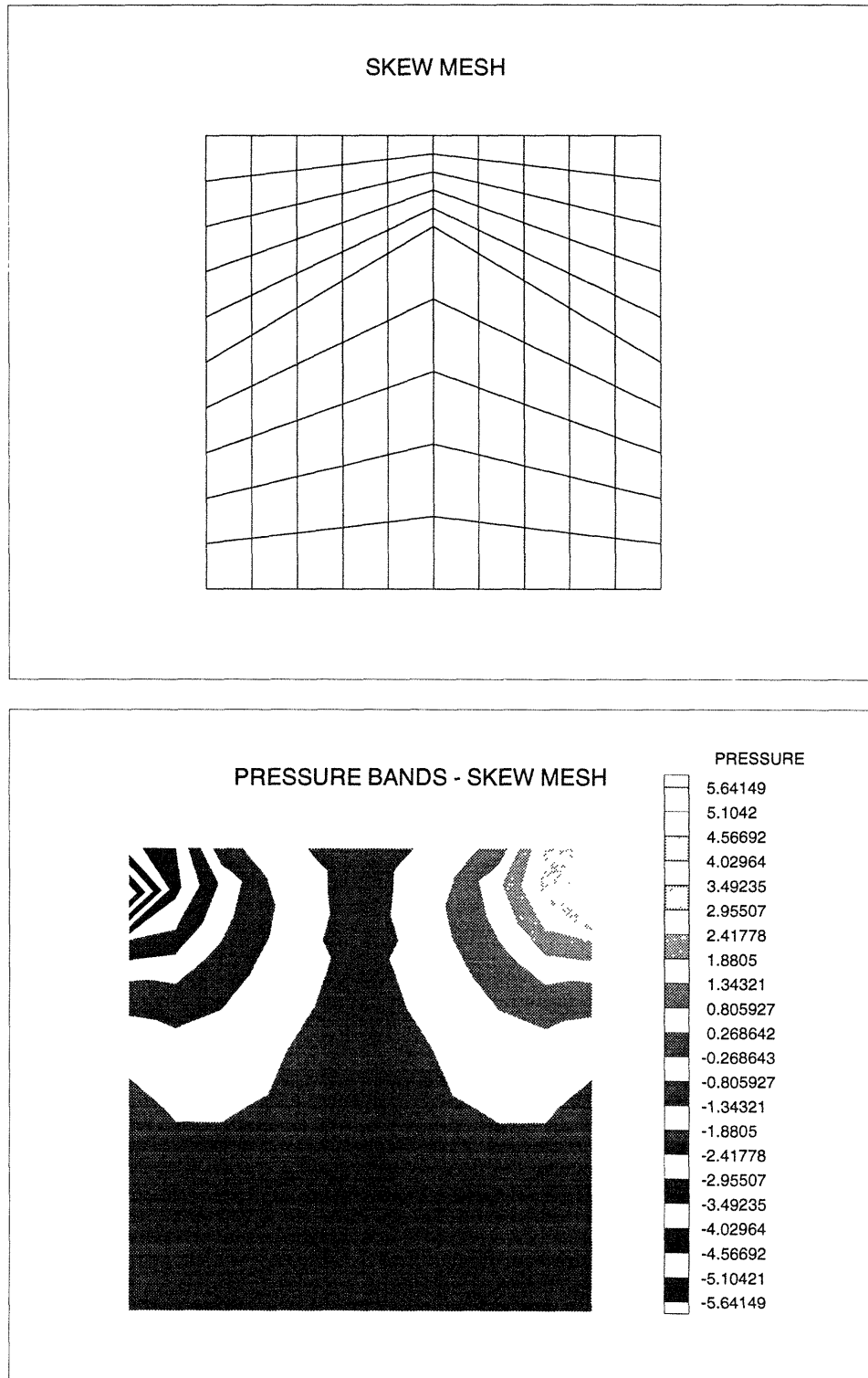


Figure 5-4: Driven cavity. Pressure bands

5.4 Convergence analysis

To study the rate of convergence of our new element we have implemented an ad-hoc test problem which is free of boundary singularities. Indeed, we prescribed a displacement field such that it vanishes and the stress field presents no singularities along the boundaries of the model considered. The displacement field is defined by

$$u = (x - x^2)(y - y^2) e^{ky} \cos(2kx) \quad (5.1)$$

$$v = (x - x^2)(y - y^2) e^{ky} \sin(2kx) \quad (5.2)$$

The stress and strain field are obtained through kinematic relations and constitutive equations respectively. The exact applied body forces are then given by,

$$f_x^B = - \left[\frac{\partial \tau_{xx}}{\partial x} + \frac{\partial \tau_{xy}}{\partial y} \right] \quad (5.3)$$

$$f_y^B = - \left[\frac{\partial \tau_{xy}}{\partial x} + \frac{\partial \tau_{yy}}{\partial y} \right] \quad (5.4)$$

We load our model with these calculated body forces to obtain the nodal displacements and the required norms

$$\| \mathbf{u} - \mathbf{u}_h \| = \| 2E - 2E_h \| \quad (5.5)$$

where E is the elastic strain energy.

We considered a sequence of meshes as shown in Figure 5-5 for non-distorted elements and in Figure 5-6 for distorted elements. The results are plotted in Figures 5-7 and 5-8 respectively. The obtained order of convergence is approximately equal to 2 as theory predicts. We also give a comparison with the results obtained using other standard finite elements.

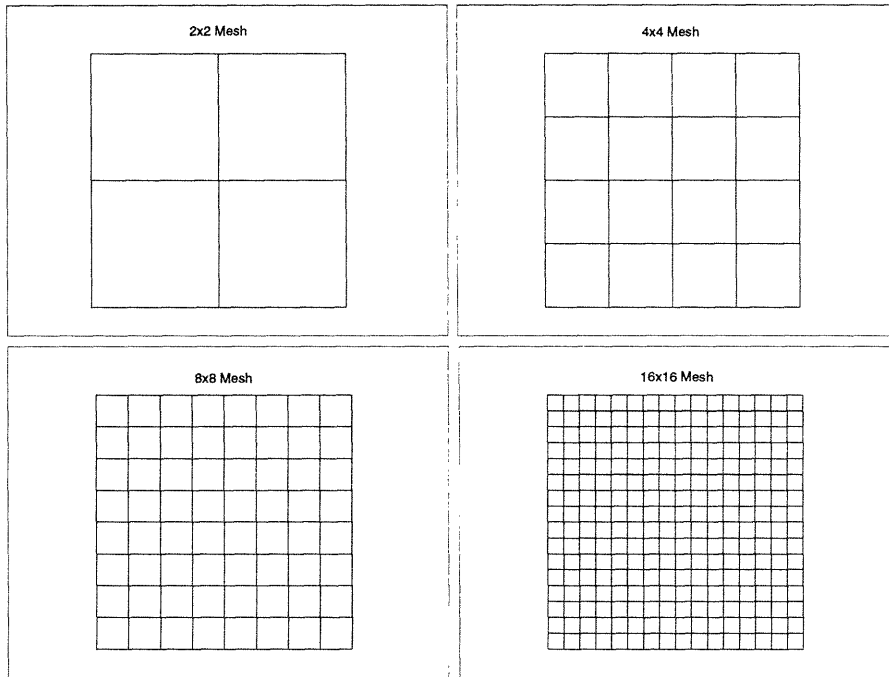


Figure 5-5: Convergence analysis. Sequence of uniform meshes considered

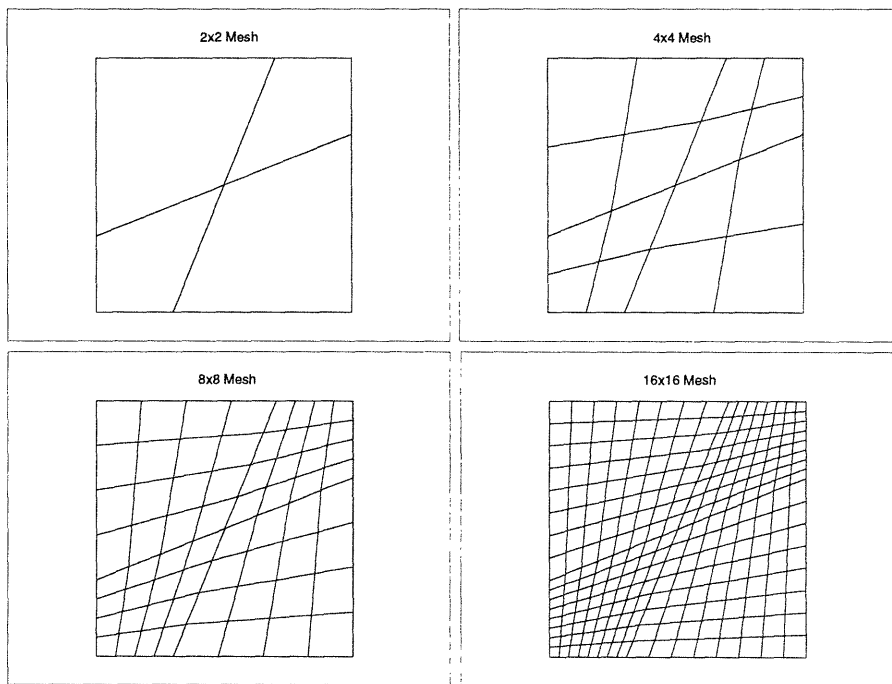


Figure 5-6: Convergence analysis. Sequence of distorted meshes considered

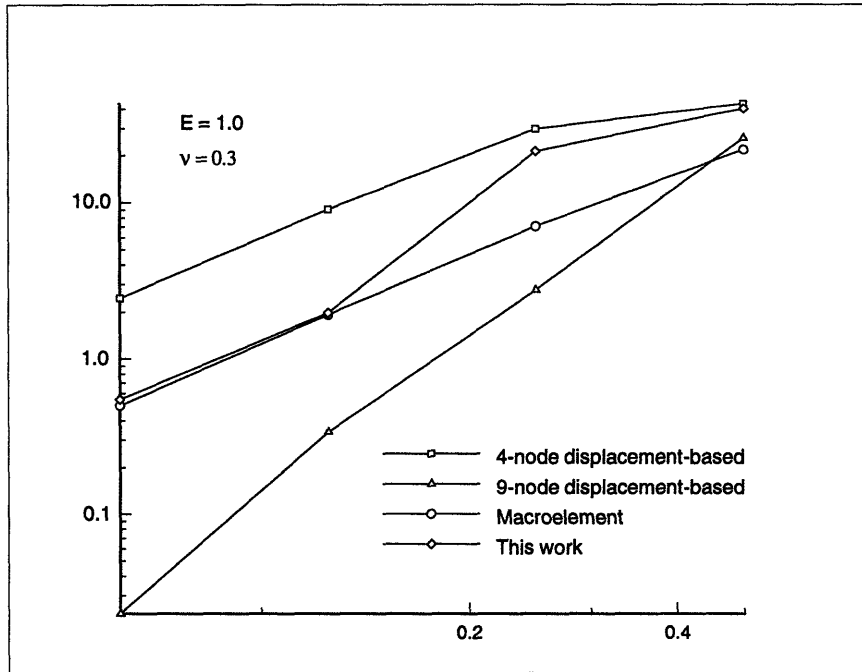


Figure 5-7: Convergence analysis. Uniform mesh results

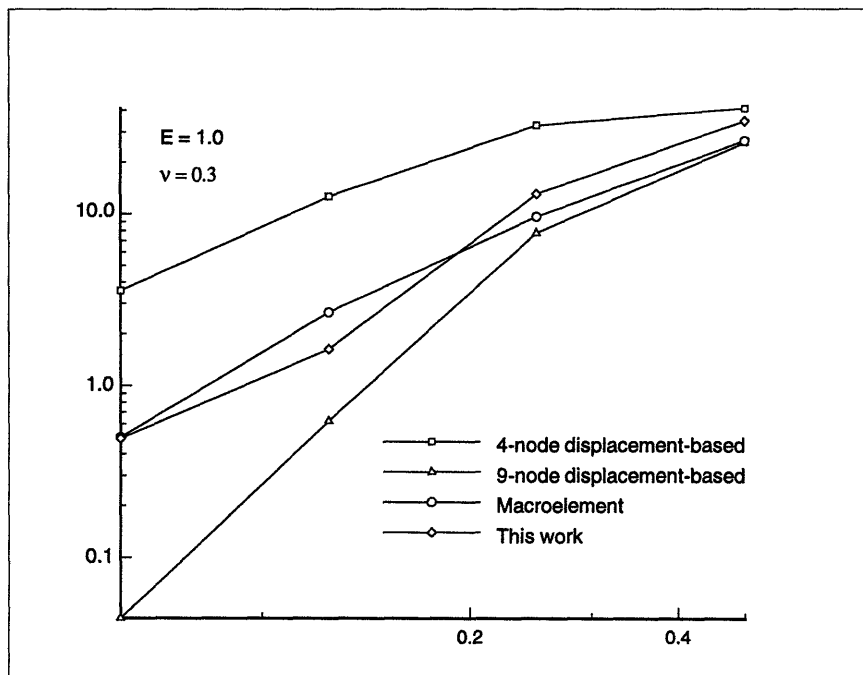


Figure 5-8: Convergence analysis. Distorted mesh results

5.5 Axisymmetric cylinder under internal pressure

To test the axisymmetric element we consider a thick cylinder of infinite length (it cannot expand in the z direction). The internal radius is $R_i = 1$ and outer radius is $R_o = 2$. The internal pressure is $p = 6$ and the Young's modulus is $E = 1000$. The analytical solution for this problem is

$$u = \frac{(1 + \nu) p R_i^2}{E (R_o^2 - R_i^2)} \left[\frac{R_o^2}{r} + (1 - 2\nu) r \right] \quad (5.6)$$

$$p = \frac{2 p R_i^2 (1 + \nu)}{3 (R_i^2 - R_o^2)} \quad (5.7)$$

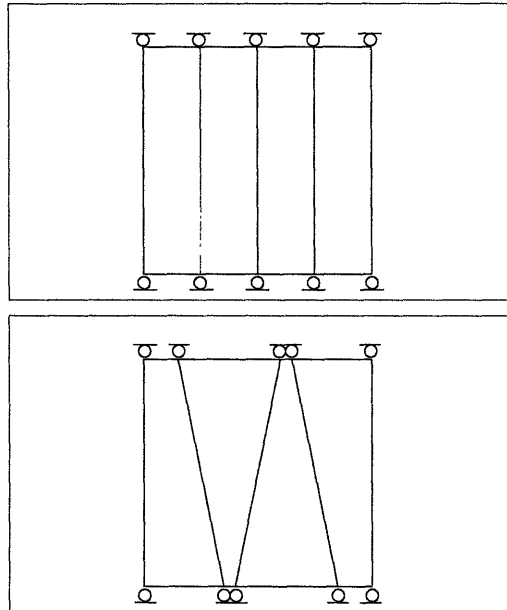


Figure 5-9: Cylinder under internal pressure. Model considered

We show in Figure 5-9 the two meshes used and in table 5-1 we list the results obtained with both meshes and the analytical results for different values of the Poisson's

ratio.

Table 5-1: Cylinder under internal pressure. Results

Displacement at $r = 0 \times 10^{-2}$			
ν	Regular mesh	Skewed mesh	Exact
0.0	0.99686	0.99566	1.000
0.3	1.13919	1.13472	1.144
0.49	1.19138	1.18920	1.198
0.4999	1.19327	1.19108	1.199

We also studied the rates of convergence using this rather simple case with a Poisson's ratio $\nu = 0.4999$. Figure 5-10 shows the L_2 norms of the analytical displacement minus the finite element displacement and the analytical pressure minus the finite element pressure as a function of the mesh size h .

We note that in this analysis, the proposed element converges with order 2 in the displacement norm and an order larger than 1 in the pressure norm. It is also interesting to compare the performance with the convergence of the 9/4-c element (the Q2-Q1 element) and the displacement-based element. The order of displacement convergence of both 9-node elements is 3, but the error using the displacement-based element is much larger. Considering that $\| \mathbf{u} - \mathbf{u}_h \|_0 \doteq c h^3$, this error is due to a large constant c , typical of the locking behavior.

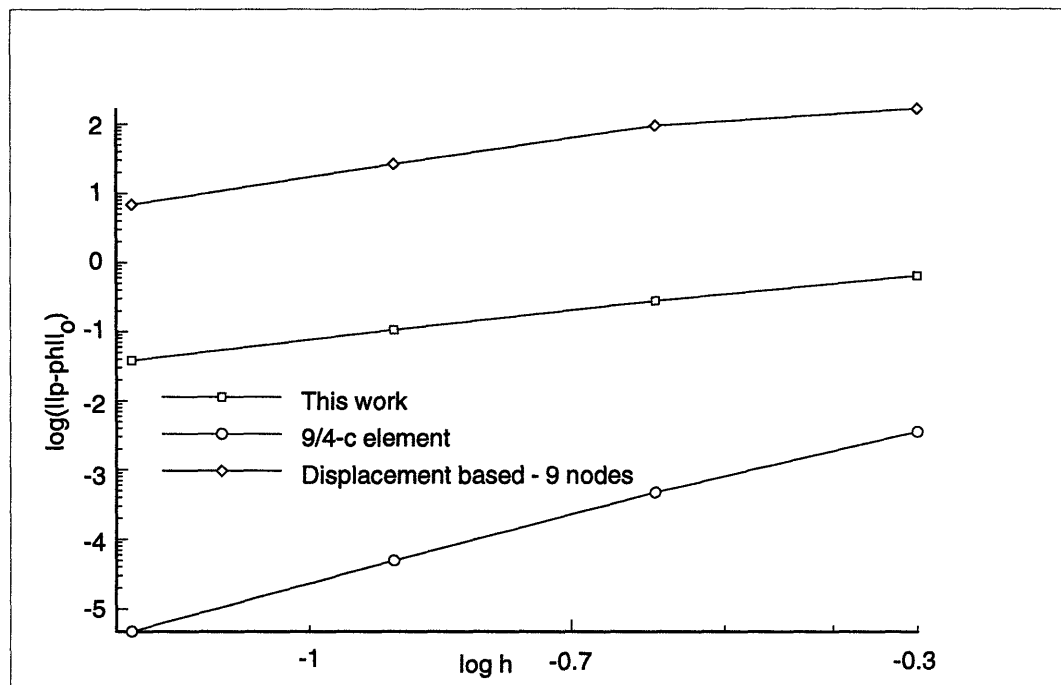
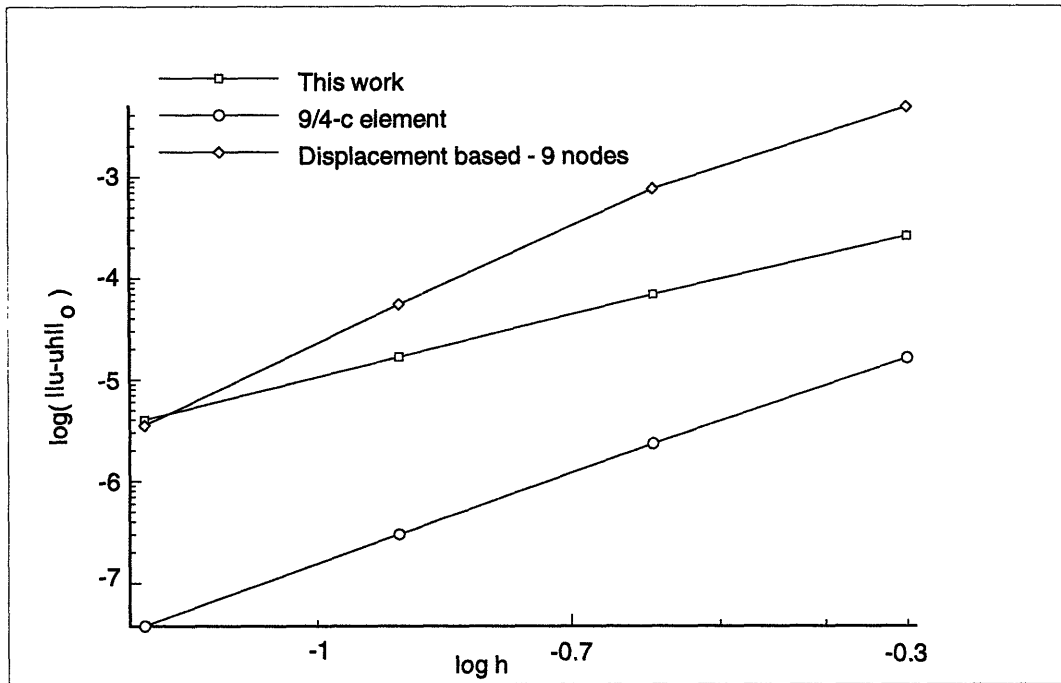


Figure 5-10: Cylinder under internal pressure. Convergence rates

5.6 Thin cylinder under bending action

The behavior of the axisymmetric element under bending action is tested in this case. A cylindrical shell of median radius $R = 167.5$, height $h = 51$ and thickness $t = 1$ is considered. The Young's modulus is $E = 11250$ and a moment $M = 2000$ is applied at one end. The shell is clamped at the other end as shown in Figure 5-11.

The analytical results are given by

$$w_{top} = \frac{M}{2 \beta^2 D}; \quad \beta^4 = \frac{E t}{4 R^2 D}; \quad D = \frac{E t^3}{12(1 - \nu^2)} \quad (5.8)$$

and the obtained results are listed in table 5-2

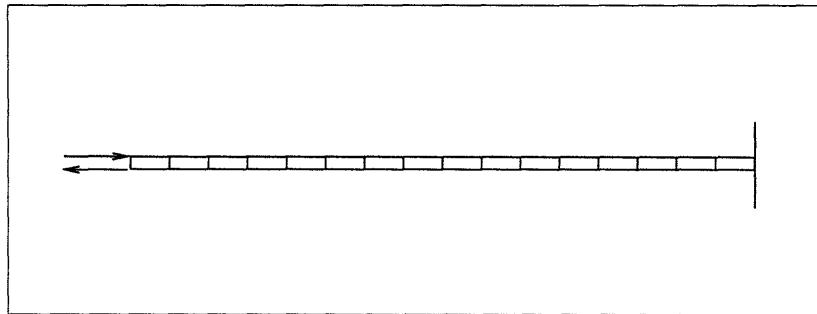


Figure 5-11: Thin cylinder under bending action. Model considered

Table 5-2: Thin cylinder under bending action. Results

Top displacement		
ν	Model	Exact
0.0	0.60536	0.6158
0.3	0.57778	0.5875
0.49	0.52857	0.5368
0.4999	0.52519	0.5334

5.7 Circular plate under uniformly distributed load

A circular plate of radius $R = 10$ and thickness $t = 1$ is subjected to a uniformly distributed load $q = 1$. The Young's modulus is $E = 1875$ and the exact solution for the central displacement is given by

$$w_{max} = \frac{q R^4}{64 D} \left(\frac{5 + \nu}{1 + \nu} + \frac{4}{3} \frac{3 + \nu}{1 - \nu^2} \frac{t^2}{R^2} \right); \quad D = \frac{E t^3}{12(1 - \nu^2)} \quad (5.9)$$

Figure 5-12 shows the mesh used and the results are given in table 5-3.

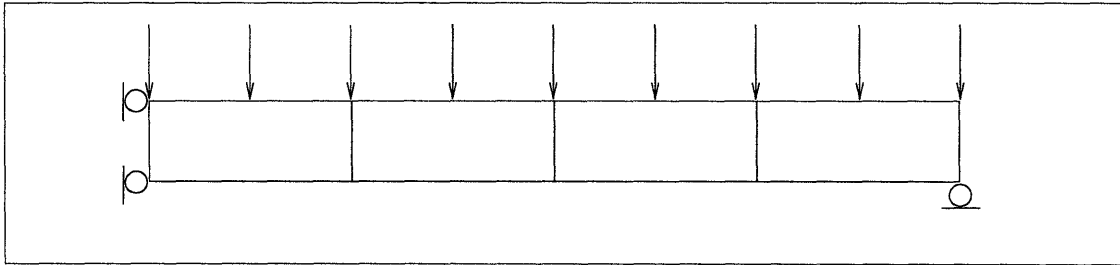


Figure 5-12: Circular plate under uniformly distributed load. Model considered

Table 5-3: Circular plate under uniformly distributed load. Results

Central displacement		
ν	Model	Exact
0.0	5.3192	5.0320
0.3	4.1440	3.7436
0.49	3.3330	2.8248
0.4999	3.2863	2.7855

Chapter 6

Three-dimensional analysis

We extend in this chapter our element presented in chapter 4 to three-dimensional analysis and present some numerical results.

6.1 The three-dimensional element

Low order three-dimensional models present, generally, the same difficulties that we have discussed in previous chapters for two-dimensional analysis. Furthermore, the computational cost is critical and the use of higher order elements is very expensive. As for the case of two-dimensional analysis, Q1/P0 elements fail to satisfy the inf-sup condition and we refer again to [10] for further details. Also, see [21] for a discussion in the context of assumed strain fields.

We obtain here our three-dimensional element as a natural extension of the element presented in chapter 4 for two-dimensional analysis. The element is based on the same variational formulation and therefore, we use eqns. (4.16) to obtain our governing finite element equations.

The three-dimensional element has eight corner nodes used for the coordinate, displacement and pressure interpolations,

$$\begin{aligned}
\mathbf{x} &= \sum_{i=1}^8 h_i(\mathbf{r}) \mathbf{x}_i \\
\mathbf{u} &= \sum_{i=1}^8 h_i(\mathbf{r}) \mathbf{u}_i \\
p &= \sum_{i=1}^8 h_i(\mathbf{r}) p_i
\end{aligned} \tag{6.1}$$

Again, the selection of the interpolation for the enhanced strain field plays a crucial role. The requirements to be satisfied by this interpolation are the same as those discussed for the quadrilateral element. We now consider, as before, the 2x2x2 undistorted element and define,

$$\mathbf{G}^*(\mathbf{r}) = \begin{bmatrix} r & 0 & 0 & 0 & 0 & 0 & 0 & 0 & 0 & 0 & rs & 0 & 0 & rt & 0 & 0 \\ 0 & s & 0 & 0 & 0 & 0 & 0 & 0 & 0 & 0 & 0 & sr & 0 & 0 & st & 0 \\ 0 & 0 & t & 0 & 0 & 0 & 0 & 0 & 0 & 0 & 0 & 0 & tr & 0 & 0 & ts \\ 0 & 0 & 0 & r & s & 0 & 0 & 0 & 0 & 0 & 0 & 0 & 0 & 0 & 0 & 0 \\ 0 & 0 & 0 & 0 & 0 & r & t & 0 & 0 & 0 & 0 & 0 & 0 & 0 & 0 & 0 \\ 0 & 0 & 0 & 0 & 0 & 0 & 0 & s & t & 0 & 0 & 0 & 0 & 0 & 0 & 0 \end{bmatrix} \tag{6.2}$$

For a general distorted element, the enhanced strain interpolation operator is obtained in the physical coordinate system from the isoparametric coordinate system by equation (4.28). In this case,

$$\bar{\mathbf{X}}_0^{-1} = \begin{bmatrix}
X_{011}^2 & X_{021}^2 & X_{031}^2 & X_{011}X_{021} \\
X_{012}^2 & X_{022}^2 & X_{032}^2 & X_{012}X_{022} \\
X_{013}^2 & X_{023}^2 & X_{033}^2 & X_{013}X_{023} \\
2X_{011}X_{012} & 2X_{021}X_{022} & 2X_{031}X_{032} & X_{011}X_{022} + X_{012}X_{021} \\
2X_{011}X_{013} & 2X_{021}X_{023} & 2X_{031}X_{033} & X_{011}X_{023} + X_{013}X_{021} \\
2X_{012}X_{013} & 2X_{022}X_{023} & 2X_{032}X_{033} & X_{012}X_{023} + X_{013}X_{022} \\
X_{011}X_{031} & X_{021}X_{031} \\
X_{012}X_{032} & X_{022}X_{032} \\
X_{013}X_{033} & X_{023}X_{033} \\
X_{011}X_{032} + X_{012}X_{031} & X_{021}X_{032} + X_{022}X_{031} \\
X_{011}X_{033} + X_{013}X_{031} & X_{021}X_{033} + X_{023}X_{031} \\
X_{012}X_{033} + X_{013}X_{032} & X_{022}X_{033} + X_{023}X_{032}
\end{bmatrix} \quad (6.3)$$

where \mathbf{X}_0 is defined in eqn. (4.29).

6.2 Numerical results

6.2.1 Patch test

We performed the patch test shown in Figure 6-1 and the element passes this test.

6.2.2 Beam bending

This is a similar problem to the one presented in section 5.1 for 2-dimensional analysis.

We distorted the elements according to the patterns shown in Figure 6-2 and also plot the corresponding results.

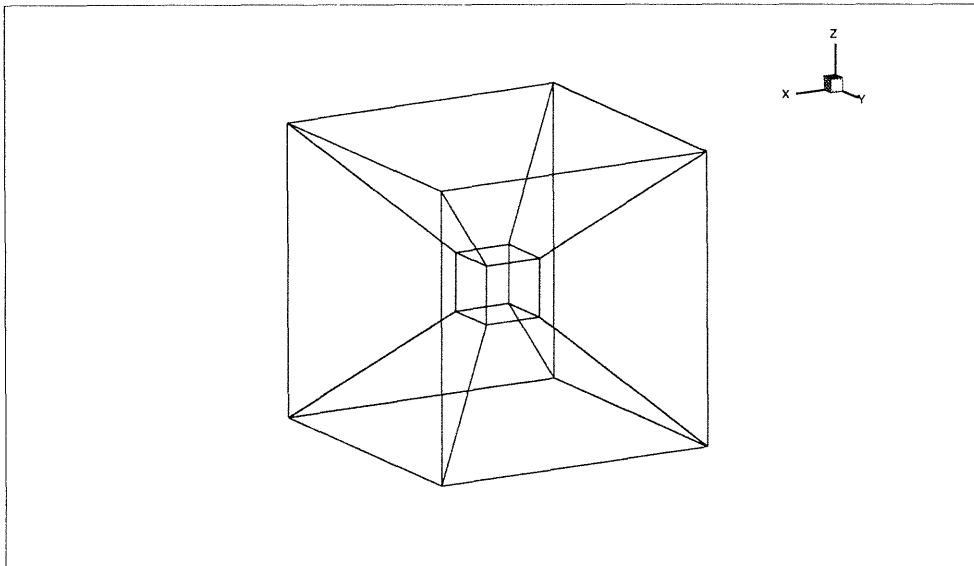


Figure 6-1: Patch test for 3-D analysis

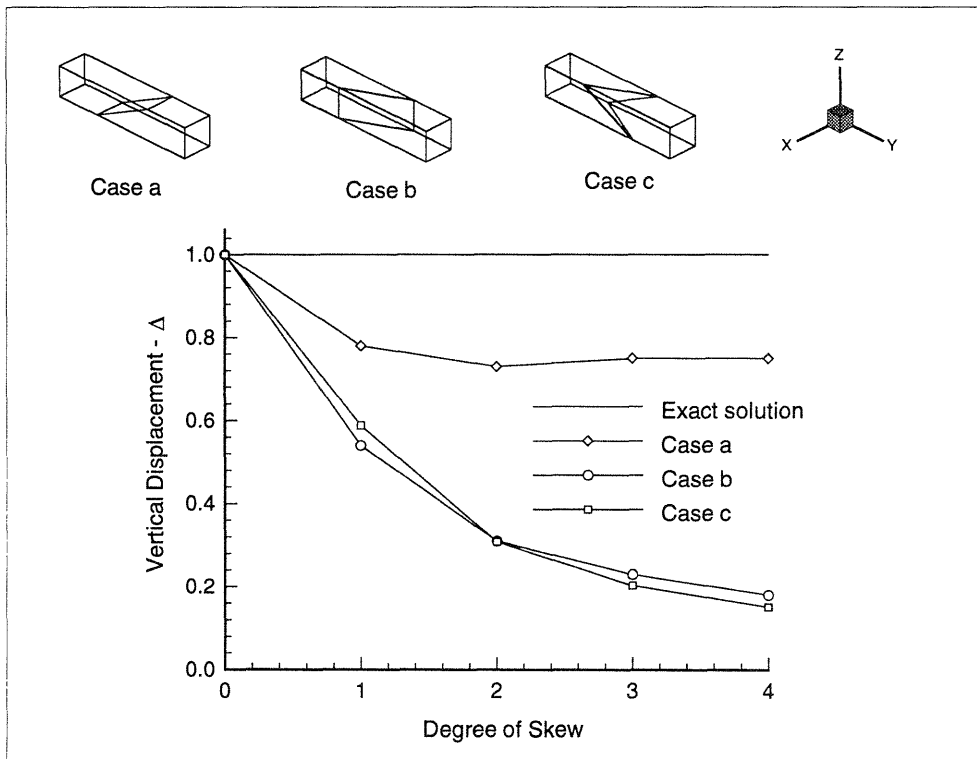


Figure 6-2: Bending test for 3-D analysis. Poisson's ratio = 0

Chapter 7

Conclusions

The main objective of this thesis was to develop a low order element with good predictive capabilities in structural bending problems and in the analysis of almost incompressible media (solids and fluids). The results presented in Chapter 5 for various test problems show the behavior of the element. The element behaves well when subjected to bending action (beam bending test) and also when almost incompressible conditions are encountered (no-flow test and driven cavity test). Furthermore, results do not deteriorate drastically when the element is subjected to large distortions.

The optimal rate of convergence, as theory predicts, was obtained for the displacement in numerical tests. On the other hand, the rate of convergence for pressure lies between 1 and 2. A numerical inf-sup test was also implemented and the element passes this test.

We have extended in Chapter 6 the proposed element to three-dimensional analysis. It was straight forwardly obtained from the two-dimensional element. However, more work must be done to obtain an improvement when the element is subjected to different types of distortions.

We also reported other possibilities for the selection of the interpolation fields. We explained in detail why other strain fields do not yield improvements in the element behavior. We also showed that, in the context presented in chapter 4, the

use of constant pressure interpolation and an enhancement of the strain field always leads to the presence of spurious pressure modes. We consider that this section has relevant importance since it gives some insight for future developments based on mixed interpolations of strain and pressure fields.

References

- [1] K. J. Bathe. *Finite Element Procedures*. Prentice Hall, Inc., Englewood Cliffs, New Jersey, 1995.
- [2] T.J.R. Hughes. Generalization of selective integration procedures to anisotropic and nonlinear media. *International Journal for Numerical Methods in Engineering*, 15:1413–1418, 1980.
- [3] K.J. Bathe and E.N. Dvorkin. A formulation of general shell elements - the use of mixed interpolation of tensorial components. *International Journal for Numerical Methods in Engineering*, 22:697–722, 1986.
- [4] E.N. Dvorkin and S.I. Vasolo. A quadrilateral 2d finite element based on mixed interpolation of tensorial components. *Engineering Computations*, 6:217–224, 1989.
- [5] J.C. Simo and M.S. Rifai. A class of mixed assumed strain methods and the method of incompatible modes. *International Journal for Numerical Methods in Engineering*, 29:1595–1638, 1990.
- [6] T.H.H. Pian and K. Sumihara. Rational approach for assumed stress finite elements. *International Journal for Numerical Methods in Engineering*, 20:1685–1695, 1984.

-
- [7] E.F. Punch and S.N. Atluri. Development and testing of stable, invariant, isoparametric curvilinear 2- and 3-d hybrid-stress elements. *Computer Methods in Applied Mechanics and Engineering*, 47:331–356, 1984.
- [8] F. Brezzi and J. Pitkaranta. On the stabilization of finite element approximations of the Stokes equations. In W. Hackbush, editor, *Efficient Solutions of Elliptic Systems. Notes on Numerical Fluid Mechanics*, 10. Brunnschweig, Wiesbaden, Vieweg, 1984.
- [9] U. Hueck and H.L. Schreyer. The use of orthogonal projections to handle constraints with applications to incompressible four-node quadrilateral elements. *International Journal for Numerical Methods in Engineering*, 35:1633–1661, 1992.
- [10] F. Brezzi and M. Fortin. *Mixed and Hybrid Finite Element Methods*. Springer-Verlag, 1991.
- [11] D. Chapelle and K.J. Bathe. The inf-sup test. *Computers & Structures*, 47(4/5):537–545, 1993.
- [12] T.J.R. Hughes, L.P. Franca and M. Balestra. A new finite element formulation of computational fluid dynamics: V. Circumventing the Babuška-Brezzi condition: A stable Petrov-Galerkin formulation of the Stokes problem accomodating equal-order interpolations. *Computer Methods in Applied Mechanics and Engineering*, 59:85–99, 1986.
- [13] O.C. Zienkiewicz and J. Wu. Incompressibility without tears - how to avoid restrictions of mixed formulations. *International Journal for Numerical Methods in Engineering*, 32:1189–1203, 1991.
- [14] E.L. Wilson and A. Ibrahimbegovic. Use of incompatible displacement modes for the calculation of element stiffness and stresses. *Finite Elements in Analysis and Design*, 7:229–241, 1990.

-
- [15] J.C. Simo and T.J.R. Hughes. On the variational foundations of assumed strain methods. *Journal of Applied Mechanics, ASME*, 53:51–54, 1986.
- [16] G. Strang. *Linear Algebra and Its Applications*. Harcourt Brace Jovanovich, San Diego, third edition, 1988.
- [17] P. G. Ciarlet. *The Finite Element Method for Elliptic Problems*. North Holland, Amsterdam, 1978.
- [18] F. Brezzi and K.J. Bathe. The inf-sup condition, equivalent forms and applications. In K.J. Bathe and D.R.J. Owen, editors, *Reliability of Methods for Engineering Analysis*, pages 197–219. Pineridge, Swansea., 1986.
- [19] D.S. Malkus and E.T. Olsen. Obtaining error estimates for optimally constrained incompressible finite elements. *Computer Methods in Applied Mechanics and Engineering*, 45:331–353, 1984.
- [20] L.P. Franca and C. Farhat. On the limitations of bubble functions. *Computer Methods in Applied Mechanics and Engineering*, 117:225–230, 1994.
- [21] F. Armero J.C. Simo and R.L. Taylor. Improved versions of assumed enhanced strain tri-linear elements for 3-d finite deformation problems. *Computer Methods in Applied Mechanics and Engineering*, 110:359–386, 1993.